

Accuracy of macroscopic and microscopic pK_a predictions of small molecules evaluated by the SAMPL6 Blind Challenge

Mehtap Isik (ORCID: 0000-0002-6789-952X)^{1,2*}, Ariën S. Rustenburg (ORCID: 0000-0002-3422-0613)^{1,3}, Andrea Rizzi (ORCID: 0000-0001-7693-2013)^{1,4}, M. R. Gunner⁶, David L. Mobley (ORCID: 0000-0002-1083-5533)⁵, John D. Chodera (ORCID: 0000-0003-0542-119X)¹

¹Computational and Systems Biology Program, Sloan Kettering Institute, Memorial Sloan Kettering Cancer Center, New York, NY 10065, United States; ²Tri-Institutional PhD Program in Chemical Biology, Weill Cornell Graduate School of Medical Sciences, Cornell University, New York, NY 10065, United States; ³Graduate Program in Physiology, Biophysics, and Systems Biology, Weill Cornell Medical College, New York, NY 10065, United States; ⁴Tri-Institutional PhD Program in Computational Biology and Medicine, Weill Cornell Graduate School of Medical Sciences, Cornell University, New York, NY 10065, United States; ⁵Department of Pharmaceutical Sciences and Department of Chemistry, University of California, Irvine, Irvine, California 92697, United States; ⁶Department of Physics, City College of New York, New York NY 10031

***For correspondence:**
mehtap.isik@choderlab.org (MI)

17

Abstract

Acid dissociation constant (pK_a) prediction is a prerequisite for predicting many other properties of small molecules such as protein-ligand binding affinity, distribution coefficient ($\log D$), membrane permeability, and solubility due to the necessity of predicting relevant protonation states and the free energy penalty of each state. SAMPL6 pK_a Challenge was the first time that a separate challenge was conducted for evaluating pK_a predictions as a part of SAMPL. It was motivated by the inaccuracies observed in prior physical property prediction challenges, such as SAMPL5 $\log D$ Challenge, caused by protonation state and pK_a prediction issues. The goal of the pK_a challenge was to elucidate the performance of contemporary pK_a prediction methods for drug-like molecules. The challenge set was composed of 24 kinase inhibitor fragment-like small molecules and some of them were multiprotic. 11 research groups contributed blind prediction sets of 37 pK_a prediction methods. Four widely used pK_a prediction methods that were missing from blind predictions were added as reference methods to challenge analysis. Collecting both microscopic and macroscopic pK_a predictions allowed in-depth evaluation of pK_a prediction performance. This article highlights deficiencies of typical pK_a prediction evaluation approaches when the difference between microscopic and macroscopic pK_a s is ignored and suggests more stringent evaluation criteria for microscopic and macroscopic pK_a predictions guided by the available experimental data. Top-performing submissions for macroscopic pK_a predictions achieved RMSE of 0.7-1.0 units and included both quantum-mechanical and empirical approaches. These predictions included less than 8 extra/missing macroscopic pK_a s for the set of 24 molecules. A large number of submissions had RMSE spanning 1-3 pK_a units. Molecules with sulfur-containing heterocycles, iodo, and bromo groups suffered from less accurate pK_a predictions on average considering all methods evaluated. For a subset of molecules, the available NMR-based dominant microstate sequence data was utilized to elucidate dominant tautomer prediction errors of microscopic pK_a predictions which was prominent for charged tautomers. SAMPL6 pK_a Challenge demonstrated the need for improving pK_a prediction methods for drug-like molecules, especially for challenging moieties and multiprotic molecules. The level of pK_a prediction inaccuracy observed in this challenge has potential to be detrimental to the performance of protein-ligand binding affinity predictions in two ways: (1) errors in predicted dominant charge and tautomeric state and (2) errors in the calculation of free energy correction for minor and multiple protonation states of the ligand.

43 0.1 Keywords

44 SAMPL · blind prediction challenge · acid dissociation constant · pK_a · small molecule · macroscopic pK_a · microscopic pK_a · macro-
45 scopic protonation state · microscopic protonation state

46 0.2 Abbreviations

47 **SAMPL** Statistical Assessment of the Modeling of Proteins and Ligands

48 **pK_a** $-\log_{10}$ acid dissociation equilibrium constant

49 **SEM** Standard error of the mean

50 **RMSE** Root mean squared error

51 **MAE** Mean absolute error

52 τ Kendall's rank correlation coefficient (Tau)

53 **R²** Coefficient of determination (R-Squared)

54 1 Introduction

55 The acid dissociation constant (pK_a) describes the protonation state equilibrium of a molecule given pH. Predicting pK_a is a
56 prerequisite for predicting many other properties of small molecules such as protein-ligand binding affinity, distribution coeffi-
57 cient ($\log D$), membrane permeability, and solubility. Computer-aided drug design efforts include assessing properties of virtual
58 molecules to guide synthesis and prioritization decisions. In such cases an experimental pK_a measurement is not possible.
59 Therefore, accurate computational pK_a prediction methods are required.

60 For a monoprotic weak acid (HA) or base (B) dissociation equilibria shown in Equation 1, the acid dissociation constant is
61 expressed as in Equations 2 or its common negative logarithmic form as in Equation 3. The ratio of ionization states can be
62 calculate with HHenderson-Hasselbalch equations shown in Equation 4.



$$K_a = \frac{[A^-][H^+]}{[HA]} \quad K_a = \frac{[B][H^+]}{[BH^+]} \quad (2)$$

$$pK_a = -\log_{10} K_a \quad (3)$$

$$pH = pK_a + \log_{10} \frac{[A^-]}{[HA]} \quad pH = pK_a + \log_{10} \frac{[B]}{[BH^+]} \quad (4)$$

63 Ionizable sites are found often in drug molecules and influence their pharmaceutical properties including target affinity,
64 ADME/Tox, and formulation properties [1]. Drug molecules with titratable groups can exist in many different charge and proto-
65 nation states based on the pH of the environment. We rely on pK_a values to determine in which charge and protonation states
66 the molecules exists and relative populations of these states. The pH of the human gut ranges between 1-8 and 74% of approved
67 drugs can change ionization states withing this physiological pH range [2] and because of this pK_a values of drug molecules pro-
68 vides essential information about their physicochemical and pharmaceutical properties. A wide distribution of acidic and basic
69 pK_a values, ranging from 0 to 12, have been observed in approved drugs [1, 2].

70 Small molecule pK_a predictions influence computational protein-ligand binding affinities in multiple ways. Errors in pK_a pre-
71 dictions can cause modeling the wrong charge, protonation, and tautomerization states which affect hydrogen bonding oppor-
72 tunities and charge distribution of the ligand. The prediction of the dominant protonation state and relative population of minor
73 states in aqueous medium is dictated by the pK_a values. The relative free energy of different protonation states in the aque-
74 ous state is a function of pK_a and pH, it contributes to the overall protein-ligand affinity in the form of a free energy penalty of
75 reaching higher energy protonation states [3].

76 Drug-like molecules present difficulties for pK_a prediction compared to simple monoprotic molecules. Drug-like molecules
77 are frequently multiprotic, have large conjugated systems, heterocycles, tautomerization. In addition that larger molecules
78 with conformational flexibility can have intramolecular hydrogen bonding which shifts pK_a values. These shifts could be real or

modeling artifacts due to collapsed conformations caused by deficiencies in solvation models. Yet predicting pK_a s of drug-like molecules accurately is a prerequisite for computational drug discovery and design.

The definition of pK_a diverges into two for multiprotic molecules: macroscopic pK_a and microscopic pK_a [4–6]. Macroscopic pK_a describes the equilibrium dissociation constant between different charged states of the molecule. Each charge state can be composed of multiple tautomers. Macroscopic pK_a is about the deprotonation of the molecule, not a particular titratable group. Microscopic pK_a describes the acid dissociation equilibrium between individual tautomeric states of different charges. We refer to collection of all tautomeric states of different macroscopic states (charge states) as microscopic states. Microscopic pK_a value defined between two microstates captures the deprotonation of a single titratable group with a fixed background protonation state of other titratable groups. In molecules with multiple titratable groups, the protonation state of one group can affect the proton dissociation propensity of another functional group, therefore the same titratable group may have different microscopic pK_a values based on the protonation state of the rest of the molecule. Different experimental methods capture different definitions of pK_a s as explained in more detail in this prior publication [7]. Most common pK_a measurement techniques such as potentiometric and spectrophotometric methods measure macroscopic pK_a s while NMR measurements can determine microscopic pK_a s and microstate populations. Therefore, it is important to pay attention to the source and definition of pK_a values to interpret their meaning correctly. Computational methods can predict both microscopic and macroscopic pK_a s. While microscopic pK_a predictions are more informative for determining relevant microstates/tautomers of a molecule and their relative free energies, computing predicted macroscopic pK_a s is useful for direct comparison of methods to more common macroscopic experimental measurements. In this paper, we explore approaches to assess the performance of both macroscopic and microscopic pK_a predictions, taking advantage of available experimental data.

1.1 Motivation for a blind pK_a challenge

SAMPL (Statistical Assessment of the Modeling of Proteins and Ligands) is a series of annual computational prediction challenges for the computational chemistry community. The goal of SAMPL is evaluate to current performance of the models and to bring the attention of quantitative biomolecular modeling field on major issues that limit the accuracy of protein-ligand binding models.

SAMPL Challenges that focus on different physical properties so far have assessed intermolecular binding models of various protein-ligand and host-guest systems, solvation models to predict hydration free energies and distribution coefficients. Potential benefits of these challenges are motivating improvement computational methods and revealing unexpected contributors to error by focusing on interesting test systems. SAMPL Challenges have demonstrated the effects of force field accuracy, sampling issues, solvation modeling defects, and tautomer/protonation state predictions on protein-ligand binding predictions.

During the SAMPL5 log D Challenge, the performance of cyclohexane-water log D predictions were lower than expected and accuracy suffered when protonation states and tautomers were not taken into account [8, 9]. With the motivation of deconvoluting the different sources of error contributing to the large errors observed in the SAMPL5 log D Challenge, we organized separate of pK_a and log P challenges in SAMPL6 [7, 10, 11]. For this iteration of the SAMPL challenge, we have taken one step back and isolated just the problem of predicting aqueous protonation states.

This is the first time a blind pK_a prediction challenge has been fielded as part of SAMPL. In this first iteration of the challenge, we aimed to assess the performance of current pK_a prediction methods for drug-like molecules, investigate potential causes of inaccurate pK_a estimates, and determine how much current level of expected accuracy might impact protein binding affinity predictions. In binding free energy predictions, any error in predicting the free energy of accessing a minor aqueous protonation state of ligand that contributes to the complex formation will directly add to the error in the predicted binding free energy. Similarly for log D predictions, inaccurate prediction aqueous protonation state that contribute partitioning between phases or prediction of relative free energy of these states will be detrimental to the accuracy of transfer free energy predictions.

1.2 Approaches to predict small molecule pK_a s

Overview of kinds of pK_a prediction methods available. Define method categories: DL, LFER, QSPR/ML, QM, QM+LEC, and QM+MM

2 Methods

2.1 Design and logistics of the SAMPL6 pK_a Challenge

The SAMPL6 pK_a Challenge was conducted as a blind prediction challenge focus on predicting aqueous pK_a value of 24 small molecules that resemble fragments of kinase inhibitors. The compound selection process was described in depth in the prior

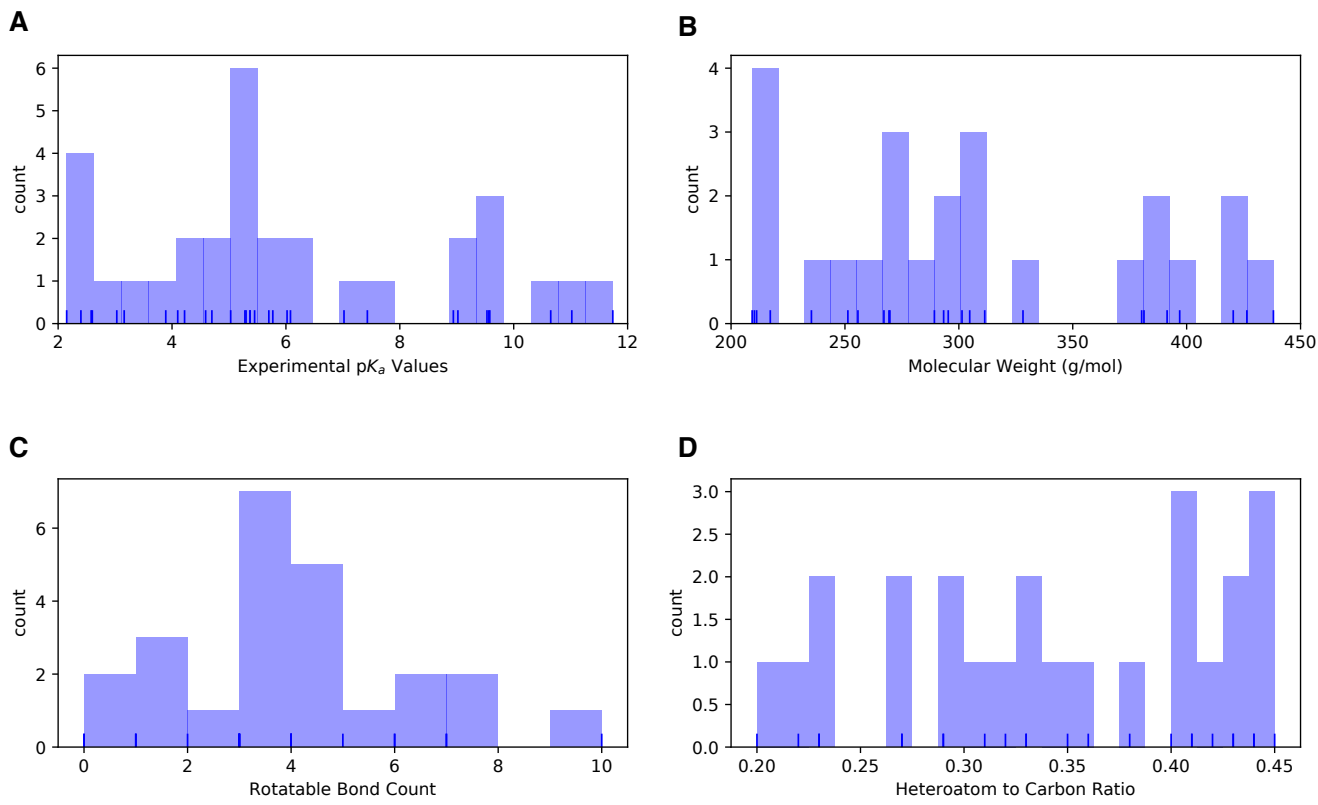


Figure 1. Distribution of molecular properties of 24 compounds in SAMPL6 pK_a Challenge. **A** Histogram of spectrophotometric pK_a measurements collected with Sirius T3 [7]. Overlayed carpet plot indicates the actual values. Five compounds have multiple measured pK_a s in the range of 2-12. **B** Histogram of molecular weights of compounds in SAMPL6 set. Molecular weights were calculated by neglecting counter ions. **C** Histogram of the number of non-terminal rotatable bonds in each molecule. **D** The histogram of the ratio of heteroatom (non-carbon heavy atom) count to the number of carbon atoms.

126 publication reporting SAMPL6 pK_a Challenge experimental data collection [7]. The distribution of molecular weights, experimen-
127 tal pK_a values, number of rotatable bonds, and heteroatom to carbon ratio are depicted in Fig. 1. The challenge molecule set
128 was composed of 17 small molecules with limited flexibility (less than 5 non-terminal rotatable bonds) and 7 molecules with
129 5-10 non-terminal rotatable bonds. The distribution of experimental pK_a values ranged between 2-12 and roughly uniform. 2D
130 representations of all compounds were provided in Fig. 5. Drug-like molecules are often larger and more complex than the ones
131 used in this study, however, aimed for the

132 The dataset composition and details of the pK_a measurement technique, except the identity of the small molecules, were
133 announced about a month before the challenge start time. Experimental macroscopic pK_a measurements were collected with
134 spectrophotometric method of Sirius T3, at room temperature in ionic strength-adjusted water with 0.15 M KCl [7]. The instruc-
135 tions for participation and the identity of the challenge molecules were released at the challenge start date (October 25, 2017).
136 A table of molecule IDs (in the form of SM##) and their canonical isomeric SMILES was provided as input. Blind prediction
137 submissions were accepted until January 22, 2018.

138 Following the conclusion of the blind challenge, the experimental data was made public on January 23, 2018. The SAMPL
139 organizers and participants gathered at the Second Joint D3R/SAMPL Workshop, at UC San Diego, La Jolla, CA on February 22-23,
140 2018 to share results. The workshop aimed to create an opportunity for participants to have discussions, evaluate the results
141 and lessons of the challenge together. The participants reported their results and their own evaluations in the special issue of
142 the Journal of Computer-Aided Molecular Design [12].

143 In this first iteration of pK_a prediction challenge we were not sure what was the best way to capture all necessary informa-
144 tion related to pK_a predictions. Our aim was to directly evaluate macroscopic pK_a predictions comparing them to experimental
145 macroscopic pK_a values and to use collected microscopic pK_a prediction data for more in-depth diagnostics of method perfor-
146 mance. Therefore, we asked participants to submit their predictions in three different submission types:

- 147 • **Type I:** microscopic pK_a values and related microstate pairs
- 148 • **Type II:** fractional microstate populations as a function of pH in 0.1 pH increments
- 149 • **Type III:** macroscopic pK_a values

150 For each submission type, a machine-readable submission file template was specified. For type I submissions, participants
151 were asked to report microstate ID of protonated state, microstate ID of deprotonated state, microscopic pK_a, microscopic
152 pK_a SEM. The reason and method of microstate enumeration is discussed further in Section 2.2 "Enumeration of Microstates".
153 The SEM captures the statistical uncertainty of the predicted method. Microstate IDs were preassigned identifiers for each mi-
154 crostates in the form of SM##_micro##. For type II submission, submission format included a table that started with microstate
155 ID and consecutive columns reporting natural logarithm of fractional microstate population values of each predicted microstate
156 for 0.1 pH increments between pH 2 and 12. For type III submissions participants were asked to report molecule ID, macroscopic
157 pK_a, macroscopic pK_a SEM. It was mandatory to submit predictions for all fields for each prediction, but it was not mandatory to
158 submit predictions for all the molecules or all the submission types. Although we have accepted submissions with partial sets of
159 molecules, it would have been a better choice to require predictions for all the molecules for better comparison of method per-
160 formance. The submission files also included fields for naming the method, listing the software utilized, and a free text method
161 section for the detailed documentation of each method.

162 Participants were allowed to submit predictions with multiple methods as long as they create separate submissions files.
163 Anonymous participation to the challenge was allowed, however all participant opted to make their submissions public. All blind
164 submissions were assigned a unique 5-digit alphanumeric submission ID, which will be used throughout this paper. Unique IDs
165 were also assigned when multiple submissions exists for different submission types of the same method such as microscopic
166 pK_a(type I) and macroscopic pK_a (type III). These submission IDs were also reported in the evaluation papers of participants and
167 allow cross-referencing. Submission IDs, participant provided method names, and method categories are presented in Table 1.
168 There were many instances that multiple types of submissions of the same method were provided by participants as challenge
169 instructions requested. Although each prediction set was assigned a separate submission ID we have matched the submissions
170 that originated from the same method according to the reports of the participant. Submission ID for both macroscopic (type III)
171 and microscopic (type I) pK_a predictions of each method (when exists) are shown in Table 1.

172 2.2 Enumeration of microstates

173 To capture both the pK_a value and titration position of microscopic pK_a predictions, we needed microscopic pK_a predictions to
174 be reported together with the pair of deprotonated and protonated microstates that describes the transition. String represen-

tations of molecules such as canonical SMILES with explicit hydrogens can be written, however, there can be inconsistencies between the interpretation of canonical SMILES written by different softwares and algorithms. In order to avoid complications while reading microstate structure files from different sources, we have decided that the safest route was pre-enumerating all possible microstates of challenge compounds, assigning the microstates IDs to each in the form of SM##_micro##, and require participants to report microstate pairs using the provided microstates IDs.

We enumerated an initial list of microstates with Epik and OpenEye QUACPAC and took the union of results. Microstates with Epik were generated using Schrodinger Suite v2016-4, and running Epik to enumerate all tautomers within 20 pK_a units of pH 7. For enumerating microstates with OpenEye QUACPAC, we had to first enumerate formal charges and for each charge enumerate all possible tautomers using the settings of maximum tautomer count 200, level 5, and carbonyl hybridization False. Then we created an union of all enumerated states written as canonical isomeric SMILES. Even though resonance structures correspond to different canonical isomeric SMILES they are not different microstates, therefore it was necessary to remove resonance structures that were replicates of the same tautomer. To detect resonance structures we converted canonical isomeric SMILES to InChI hashes with explicit and fixed hydrogen layer. Structures that describe the same tautomer but different resonance states lead to explicit hydrogen InChI hashes that are identical allowing replicates to be removed. The Jupyter Notebook used for the enumeration of microstates is provided in supplementary documents. Because resonance and geometric isomerism should be ignored when matching predicted structures microstate IDs (except SM20 which should be modelled as E-isomer), we provided microstate ID tables with canonical SMILES and 2D-depictions.

Despite pooling together enumerated charge states and tautomers with Epik and OpenEye QUACPAC to our surprise the microstate lists were still incomplete. A better algorithm that can enumerate all possible microstates would be very beneficial. In SAMPL6 Challenge participants came up with new microstates that were not present in the initial list that we provided. Based on participant requests we iteratively had to update the list of microstates and assign new microstate IDs. Every time we received a request, we shared the updated microstate ID lists with all the challenge participants.

A working pK_a microstate definition for this challenge was provided in challenge instructions for clarity. Physically meaningful microscopic pK_a s are defined between microstate pairs that can interconvert by single protonation/deprotonation event of only one titratable group. So, microstate pairs should have total charge difference of |1| and only one heavy atom that differs in the number of bound hydrogens, regardless of resonance state or geometric isomerism. All geometric isomer and resonance structure pairs that have the same number of hydrogens bound to equivalent heavy atoms are related to the same microstate. Pairs of resonance structures and geometric isomers (cis/trans, stereo) won't be considered as different microstates, as long as there is no change in the number of hydrogens bound to each heavy atom in these structures. Since we wanted to participants to report only microscopic pK_a s that are describe single deprotonation events (in contrast to transitions between microstates that are different in terms of two or more titratable protons), we have also provided a pre-enumerated list of allowed microstate pairs.

Provided microstate ID and microstate pair lists were intended to be used for reporting microstate IDs and to aid parsing of submissions. The enumerated lists of microstates were not created with the intent to guide computational predictions. This was clearly stated in the challenge instructions. However, we noticed that some participants still used the microstate lists as an input for their pK_a predictions as we received complaints from participants that due to our updates to microstate lists they needed to repeat their calculations. This would not have been an issue, if participants used pK_a prediction protocols that did not rely on an external pre-enumerated list of microstates as an input. None of the participants have reported this dependency in their method descriptions explicitly, therefore we can not identify which submissions have used the enumerated microstate lists as input and which ones has followed the instructions.

2.3 Evaluation approaches

Since the experimental data for the challenge was mainly composed of macroscopic pK_a values of both monoprotic and multi-protic compounds, evaluation of macroscopic and microscopic pK_a predictions was not straightforward. For only a subset of 8 molecules, dominant microstate sequence could be inferred from NMR. For the rest of the molecules the only experimental information available was the macroscopic pK_a value, while experimental data did not provide any information on which group(s) are being titrated, microscopic pK_a values, identity of associated macrostates (which charge) or microstates (which tautomers). In this comparative performance evaluation of we let the experimental data lead the challenge analysis towards various evaluation routes. To compare macroscopic pK_a predictions to experimental values we had to utilize numerical matching algorithms before we could calculate performance statistics. For the subset of molecules with experimental data about microstates, we used microstate based matching. These matching methods were described further in the next section.

225 Three types of submissions were collected during the SAMPL6 pK_a Challenge. We have only utilized type I (microscopic pK_a
226 value and microstate IDs) and type III (macroscopic pK_a value) predictions in this article. Type I submissions contained the same
227 prediction information as the the type II submissions which reported fractional population of microstates with respect to pH.

228 2.3.1 Matching algorithms for pairing predicted and experimental pK_a s

229 Macroscopic pK_a predictions can be calculated from microscopic pK_a s for direct comparison to experimental macroscopic pK_a
230 values, although there is still a remaining issue. How to match predicted macroscopic pK_a s to experimental macroscopic pK_a s
231 when there could multiple numbers of each reported for each molecule? Experimental data in this case did not provide any
232 information that would indicate the titration site, the overall charge or the tautomer composition of macrostate pairs that are
233 associated with each measured macroscopic pK_a that can guide the matching.

234 For evaluating predictions taking the experimental data as reference Fraczkiewicz et al. delinited recommendations for fair
235 comparative analysis of computational pK_a predictions [13]. In the absence any experimental information that would aid the
236 match, experimental and computational pK_a s should be matched preserving the order of pK_a values and minimizing sum of
237 absolute errors.

238 We picked Hungarian matching algorithm [14, 15] to assign experimental and predicted macroscopic pK_a s with squared error
239 cost function as suggested by Kiril Lanevskij. The algorithm is available in SciPy package (`scipy.optimize.linear_sum_assignment`) [16].
240 This matching algorithm provides optimum global assignment that minimizes linear sum of squared errors of all pairwise
241 matches. The reason to select squared error cost function instead of absolute error cost function is to avoid misordered matches,
242 For instance, for a molecule with experimental pK_a values of 4 and 6, and predicted pK_a s of 7 and 8, Hungarian matching with
243 absolute error cost function would match 6 to 7 and 4 to 9. Hungarian matching with squared error cost would match 4 to 7
244 and 6 to 9, preserving the increasing pK_a value order between experimental and predicted values. A weakness of this approach
245 would be failing to match experimental value of 6 to predicted value of 7, if that was the correct match based on underlying
246 macrostates. But underlying pair of states were unknown to us both because experimental data of the challenge did not con-
247 tain information about what charge states the transitions were happening between and also because we have not collected the
248 pair of macrostates associated with each pK_a predictions in submissions. There is no perfect solution to numerical pK_a assign-
249 ment problem, but we tried to determine the most fair way to penalize predictions based on their numerical deviation from the
250 experimental values.

251 For the analysis of microscopic pK_a predictions we adopted a different matching approach. Only for the 8 molecules, we util-
252 ized the dominant microstate sequence infered from NMR experiments to match computational predictions and experimental
253 pK_a s. We will refer to this assignment method as microstate matching, where experimental pK_a value is matched to the com-
254 putational microscopic pK_a value which was reported for the dominant microstate pair observed for each transition. We have
255 compared the results of Hungarian matching and microstate matching.

256 Inevitably the choice of matching algorithms to assign experimental and predicted values has an impact on the calculation
257 of performance statistics. We believe the Hungarian algorithm for numerical matching and microstate-based were the best
258 choices, providing the most unbiased matching without introducing assumptions outside of the experimental data.

259 2.3.2 Statistical metrics for submission performance

260 A variety of accuracy and correlation statistics were considered for analyzing and comparing performance of predictions meth-
261 ods submitted to the SAMPL6 pK_a Challenge. Calculated performance statistics of predictions were provided to participants
262 before the workshop. Details of the analysis and scripts are maintained on the SAMPL6 Github Repository (described in Section
263 5).

264 There are six error metrics reported for the numerical error of the pK_a values: the root-mean-squared error (RMSE), mean ab-
265 solute error (MAE), mean error (ME), coefficient of determination (R^2), linear regression slope (m), and Kendall's Rank Correlation
266 Coefficient (τ). Uncertainty in each performance statistic was calculated as 95% confidence intervals estimated by bootstrapping
267 over predictions with 10000 bootstrap samples. Calculated errors statistics of all methods can be found in Table S2 for macro-
268 scopic pK_a predictions and Tables S4 and S4 for microscopic pK_a predictions.

269 In addition to the numerical error aspect of the pK_a values, we have also evaluated predictions in terms of their ability to cap-
270 ture the correct macrostates (ionization states) and microstates (tautomers of each ionization state) to the extend possible from
271 the available experimental data. For macroscopic pK_a s experiments did not provide any evidence of the identity of the ionization
272 states. However, the number of ionization states indicates the number of macroscopic pK_a s that exists between experimental
273 range of 2.0-12.0. For instance, SM14 has two experimental pK_a s and therefore 3 different charge states were observed between

274 the pH range of 2.0-12.0. If a prediction reported 4 macroscopic pK_a s, it is clear that this method predicted an extra ionization
275 state. With this perspective we reported the number of unmatched experimental pK_a s (the number of missing pK_a predictions,
276 i.e. missing ionization states) and the number of unmatched predicted pK_a s (the number of extra pK_a predictions, i.e. extra
277 ionization states) after Hungarian matching. The later count was restricted to only predictions with pK_a values between 2 and
278 12, because that was the range of the experimental method. Errors in extra or missing pK_a prediction errors highlight failure to
279 predict the correct number of ionization states within a pH range.

280 For the evaluation of microscopic pK_a predictions, taking advantage of the available dominant microstate sequence data for
281 a subset of 8 compounds, we calculated the dominant microstate prediction accuracy. Dominant microstate prediction accuracy
282 is the ratio of correct dominant tautomer predictions for each charge state divided by, calculated over all ionization states of each
283 molecule. In order to extract the sequence of dominant microstates from the microscopic pK_a predictions sets, we calculated
284 the relative free energy of microstates selecting a neutral tautomer and pH 0 as reference following the Equation 5. Calculation
285 of relative free energy of microstates was explained in more detail in a previous publication [17].

286 Relative free energy of state with respect to reference state B at pH 0.0 (arbitrary pH value selected as reference) can be
287 calculated as follows:

$$\Delta G_{AB} = \Delta m_{AB} RT \ln 10 (pH - pK_a) \quad (5)$$

288 Δm_{AB} is equal to the number protons in state A minus state B. R and T indicate molar gas constant and temperature, respectively.
289 By calculating relative free energies of all predicted microstates with respect to the same reference state and pH, we were able
290 to determine the sequence of predicted dominant microstates. The dominant tautomer of each charge state was determined
291 as the the microstate with the lowest free energy in the subset of predicted microstates of each ionization state. This approach
292 is feasible because the relative free energy of tautomers of the same ionization state is independent of pH and therefore the
293 choice of reference pH is arbitrary.

294 We created a shortlist of top-performing methods for macroscopic and microscopic pK_a predictions. Top macroscopic pK_a
295 predictions were selected based on the following criteria of consistence performance among different metrics: ranking in the
296 top 10 consistently according to two error (RMSE, MAE) and two correlation metrics (R-Squared, and Kendall's Tau), and also
297 havin a combined count of less than 8 missing or extra macroscopic pK_a s for the entire molecule set (a third of the number of
298 compounds). These methods are presented in Table 2. A separate list of top performing methods were selected for microscopic
299 pK_a with the following criteria: ranking in the top 10 methods when ranked by accuracy statistics (RMSE and MAE) and perfect
300 dominant microstate prediction accuracy. These methods are presented in Table 3.

301 In addition to comparing the performance comparison of methods, we also wanted to compare pK_a prediction performance
302 on the level of molecules to determine pK_a s of which molecules in the challenge set were harder to predict considering all the
303 methods in the challenge. For this purpose, we plotted prediction error distributions of each molecule considering all prediction
304 methods. We also calculated MAE for each molecule's over all predictions as well as for predictions from each method category.

305 2.4 Reference calculations

306 Including null model as helpful in comparative performance analysis of predictive methods to establish what the performance
307 statistics look like for a baseline method for the specific dataset. Null models or null predictions employ a simple prediction
308 model which is not expected to be particularly successful, but it is useful for providing a simple point of comparison for more
309 sophisticated methods. The expectation is for more sophisticated or costly prediction methods to outperform the predictions
310 from a null model, otherwise the simpler null model would be preferable. In SAMPL6 pK_a Challenge there were two blind submissions
311 that database lookup methods that were suitable to be considered as null predictions. These methods, with submission
312 IDs 5nm4j and 5nm4j both used OpenEye pKa-Porspector database to find the most similar molecule to query molecule and
313 report its pK_a as predicted value. We acknowledge that database lookup methods with a rich experimental database presents
314 a challenging null model to beat, however, due to the accuracy level needed from pK_a predictions for computer-aided drug de-
315 sign we believe it is an appropriate performance baseline that physical and empirical pK_a prediction methods should strive to
316 perform better than.

317 We have also included additional reference calculations in the comparative analysis to provide more perspective. The meth-
318 ods we chose to include as reference calculations were missing from the blind predictions sets although they are widely used
319 methods by academia and industry. representing different methodological approaches: Schrodinger/Epik (nb007, nb008, nb010),
320 Schrodinger/Jaguar (nb011, nb013), Chemaxon/Chemicalize (nb015), and Molecular Discovery/MoKa (nb016, nb017). Epik and
321 Jaguar pK_a predictions were collected by Bas Rustenburg, Chemicalize predictions by Mehtap Isik, and MoKa predictions by

322 Thomas Fox, after the challenge deadline avoiding any alterations to the respective standard procedures of the methods and
323 guidance of the experimental date. Reference calculations were not formally blind, as experimental data of the challenge has
324 been made publically available before their collection.

325 All figures and statistics tables in this manuscript include reference calculations. As the reference calculations were not formal
326 submissions, these were omitted from formal ranking in the challenge, but we present plots in this article which show them for
327 easy comparison. These are labeled with submission IDs of the form *nb###* to allow easy recognition of non-blind reference
328 calculations.

329 **3 Results and Discussion**

330 Participation to SAMPL6 pK_a Challenge was high with 11 research groups contributing pK_a prediction sets of 37 methods. A large
331 variety of pK_a prediction methods were represented in SAMPL6 Challenge. We categorized these submissions into four method
332 categories: database lookup (DL), linear free energy relationship (LFER), quantitative structure property relationship or machine
333 learning (QSPR/ML), and quantum mechanics (QM). Quantum mechanics models were subcategorized into QM methods with
334 and without linear empirical correction (LEC), and combined quantum mechanics and molecular mechanics (QM + MM). Table 1
335 presents, method names, submission IDs, method categories, and also references of each approach. Integral equation-based
336 approaches (e.g. EC-RISM) were also evaluated under the Physical (QM) category. There were 2 DL, 4 LFER, and 5 QSPR/ML
337 methods represented in the challenge, including the reference calculations. Majority of QM calculations include linear empirical
338 corrections (22 methods in QM + LEC category), and only 5 QM methods were submitted without any empirical corrections.
339 There were 4 methods that used a mixed physical modeling approach of QM + MM.

340 The following sections present detailed performance evaluation of blind submissions and reference prediction methods for
341 macroscopic and microscopic pK_a predictions. Performance statistics of all the methods can be found in Tables S2 and S4.
342 Methods are referred to by their submission ID's which are provided in Table 1.

343 **3.1 Analysis of macroscopic pK_a predictions**

344 The performance of macroscopic pK_a predictions were analyzed by comparison to experimental pK_a values collected by the
345 spectrophotometric method via numerical matching following the Hungarian method. Overall pK_a prediction performance was
346 lower than we have hoped for. Fig. 2 shows RMSE calculated for each prediction method represented by their submission IDs.
347 Other performance statistics are depicted in Fig. 3. In both figures method categories were indicated by the color of the error
348 bars. Statistics depicted in these figures can be found in Table S2. Prediction error ranged between 0.7 to 3 pK_a units in terms of
349 RMSE, while an RMSE between 2-3 log units was observed for the majority of methods (20 out of 38 methods). Only five meth-
350 ods achieved RMSE less than 1 pK_a unit. One is QM method with COSMO-RS approach for solvation and linear empirical cor-
351 rection (*xvxzd* (DSD-BLYP-D3(BJ)/def2-TZVPD//PBEh-3c[DCOSMO-RS] + RRHO(GFN-xTB[GBSA]) + Gsolv(COSMO-RS[TZVPD]) and
352 linear fit)), and the remaining four are empirical prediction methods of LFER (*xmyhm* (ACD/pKa Classsic), *nb007* (Schrodinger/Epic
353 Scan)) and QSPR/ML categories (*gyuhx* (Simulations Plus), *nb017* (MoKa)). These five methods with RMSE less than 1 pK_a unit also
354 are the methods that have the lowest MAE. *xmyhm* and *xvxzd* were the only two methods for which the upper 95% confidence
355 interval of RMSE was lower than 1 pK_a unit.

356 In terms of correlation statistics performance of many methods have good performance, although the ranking of methods
357 change R^2 and Kendall's Tau and many methods are indistinguishable from one another considering uncertainty of the corre-
358 lation statistics. 32 out of 38 methods have R higher than and Kendall's Tau higher than 0.7 and 0.6, respectively. 8 methods have
359 R^2 higher than 0.9 and 6 methods have Kendall's Tau higher than 0.8. The overlap of these two sets are the following: *gyuhx* (Sim-
360 ulations Plus), *xvxzd* (DSD-BLYP-D3(BJ)/def2-TZVPD//PBEh-3c[DCOSMO-RS] + RRHO(GFN-xTB[GBSA]) + Gsolv(COSMO-RS[TZVPD])
361 and linear fit), *xmyhm* (ACD/pKa Classic), *ryzue* (Adiabatic scheme with single point correction: MD/M06-2X//6-311++G(d,p)//M06-
362 2X/6-31+G(d) for bases and SMD/M06-2X//6-311++G(d,p)//M06-2X/6-31G(d) for acids + thermal corrections), and *5byn6* (Adiabatic
363 scheme: thermodynamic cycle that uses gas phase optimized structures for gas phase free energy and solution phase geome-
364 tries for solvent phase free energy. SMD/M06-2X/6-31+G(d) for bases and SMD/M06-2X/6-31G(d) for acids + thermal corrections).
365 It is worth noting that the *ryzue* and *5byn6* are QM predictions without any empirical correction. Their high correlation and rank
366 correlation coefficient scores signal that with an empirical correction their accuracy based performance could improve. Indeeded,
367 the participants have showed that this is the case in their individual challenge analysis paper and achieved RMSE of 0.73 pK_a
368 units after the challenge [26].

369 Null prediction methods based on database lookup (*5nm4j* and *pwn3m*) had similar performance, roughly RMSE of 2.5 pK_a

Table 1. Submission IDs, names, category, and type for all the pK_a prediction sets. Reference calculations are labeled as $nb\#\#\#$. The method name column lists the names provided by each participant in the submission file. The “type” column indicates if submission was or a post-deadline reference calculation, denoted by “Blind” or “Reference” respectively. The methods in the table are grouped by method category and not ordered by performance.

Method Category	Method	Microscopic pK_a (Type I) Submission ID	Macroscopic pK_a (Type III) Submission ID	Submission Type	Ref.
DL	Substructure matches to experimental data in pKa OpenEye pKa Prospector Database v1.0	<i>5nm4j</i>	Null	[18]	
DL	OpenEye pKa-Prospector 1.0.0.3 with Analog Search ion identification algorithm	<i>pwn3m</i>	Null	[18]	
LFER	ACD/pKa GALAS (ACD/Percepta Kernel v1.6)	<i>v8qph</i>	<i>37xm8</i>	Blind	[19]
LFER	ACD/pKa Classic (ACD/Percepta Kernel, v1.6)		<i>xmyhm</i>	Blind	[20]
LFER	Epik Scan (Schrodinger v2017-4)		<i>nb007</i>	Reference	[21]
LFER	Epik Microscopic (Schrodinger v2017-4)		<i>nb010</i>	Reference	[21]
QSPR/ML	OpenEye Gaussian Process	<i>6tvf8</i>	<i>hytjn</i>	Blind	[9]
QSPR/ML	OpenEye Gaussian Process Resampled		<i>q3pfj</i>	Blind	[9]
QSPR/ML	S+pKa (ADMET Predictor v8.5, Simulations Plus)	<i>hdijq</i>	<i>gyuhx</i>	Blind	[22]
QSPR/ML	Chemicalize v18.23 (ChemAxon MarvinSketch v18.23)		<i>nb015</i>	Reference	[23]
QSPR/ML	Moka v3.1.3	<i>nb016</i>	<i>nb017</i>	Reference	[24, 25]
QM	Adiabatic scheme with single point correction: SMD/M06-2X//6-311++G(d,p)//M06-2X/6-31+G(d) for bases and SMD/M06-2X//6-311++G(d,p)//M06-2X/6-31G(d) for acids + thermal corrections	<i>ko8yx</i>	<i>ryzue</i>	Blind	[26]
QM	Direct scheme with single point correction: SMD/M06-2X//6-311++G(d,p)//M06-2X/6-31G(d) for bases and SMD/M06-2X//6-311++G(d,p)//M06-2X/6-31G(d) for acids + thermal corrections	<i>w4z0e</i>	<i>xikp8</i>	Blind	[26]
QM	Adiabatic scheme: thermodynamic cycle that uses gas phase optimized structures for gas phase free energy and solution phase geometries for solvent phase free energy. SMD/M06-2X/6-31+G(d) for bases and SMD/M06-2X/6-31G(d) for acids + thermal corrections	<i>wcvnu</i>	<i>5byn6</i>	Blind	[26]
QM	Vertical scheme: thermodynamic cycle that uses only gas phase optimized structures to compute gas phase and solvation free energy. SMD/M06-2X/6-31+G(d) for bases and SMD/M06-2X/6-31G(d) for acids + Thermal corrections	<i>arcko</i>	<i>w4iyd</i>	Blind	[26]
QM	Direct scheme: solution phase free energy is determined by solution phase geometries without thermodynamic cycle SMD/M06-2X/6-31+G(d) for bases and SMD/M06-2X/6-31G(d) for acids + thermal corrections	<i>wexjs</i>	<i>y75vj</i>	Blind	[26]
QM + LEC	Jaguar (Schrodinger v2017-4)	<i>nb011</i>	<i>nb013</i>	Reference	[27]
QM + LEC	CPCM/B3LYP/6-311+G(d,p) and global fitting	<i>y4wws</i>	<i>35bdm</i>	Blind	[28]
QM + LEC	CPCM/B3LYP/6-311+G(d,p) and separate fitting for neutral to negative and for positive to neutral transformations	<i>qsicn</i>	<i>p0jba</i>	Blind	[28]
QM + LEC	EC-RISM/MP2/6-311+G(d,p)-P3NI-q-noThiols-2par	<i>kxzt</i>	<i>ds62k</i>	Blind	[29]
QM + LEC	EC-RISM/MP2/cc-pVTZ-P2-q-noThiols-2par	<i>ftc8w</i>	<i>2ii2g</i>	Blind	[29]
QM + LEC	EC-RISM/MP2/6-311+G(d,p)-P2-phi-all-2par	<i>ktpj5</i>	<i>nb001</i>	Blind*	[29]
QM + LEC	EC-RISM/MP2/6-311+G(d,p)-P2-phi-noThiols-2par	<i>wuuvc</i>	<i>nb002</i>	Blind*	[29]
QM + LEC	EC-RISM/MP2/6-311+G(d,p)-P3NI-phi-all-2par	<i>2umai</i>	<i>nb003</i>	Blind*	[29]
QM + LEC	EC-RISM/MP2/6-311+G(d,p)-P3NI-phi-noThiols-2par	<i>cm2yq</i>	<i>nb004</i>	Blind*	[29]
QM + LEC	EC-RISM/MP2/6-311+G(d,p)-P2-phi-all-1par	<i>z7fhp</i>	<i>nb005</i>	Blind*	[29]
QM + LEC	EC-RISM/MP2/6-311+G(d,p)-P3NI-phi-all-1par	<i>8toyp</i>	<i>nb006</i>	Blind*	[29]
QM + LEC	EC-RISM/MP2/cc-pVTZ-P2-phi-noThiols-2par	<i>epvmk</i>	<i>tjld0</i>	Blind	[29]
QM + LEC	EC-RISM/MP2/cc-pVTZ-P2-phi-all-2par	<i>xnoe0</i>	<i>mkhqa</i>	Blind	[29]
QM + LEC	EC-RISM/MP2/cc-pVTZ-P3NI-phi-noThiols-2par	<i>4o0ia</i>	<i>mpwiy</i>	Blind	[29]
QM + LEC	EC-RISM/B3LYP/6-311+G(d,p)-P3NI-q-noThiols-2par	<i>nxaaw</i>	<i>ad5pu</i>	Blind	[29]
QM + LEC	EC-RISM/B3LYP/6-311+G(d,p)-P3NI-phi-noThiols-2par	<i>0xi4b</i>	<i>f0gew</i>	Blind	[29]
QM + LEC	EC-RISM/B3LYP/6-311+G(d,p)-P2-phi-noThiols-2par	<i>cwyk</i>	<i>np6b4</i>	Blind	[29]
QM + LEC	PCM/B3LYP/6-311+G(d,p)	<i>gdqeg</i>	<i>yc70m</i>	Blind	[29]
QM + LEC	COSMOtherm_FINE17 (COSMOtherm C30_1701, BP/TZVPD/FINE//BP/TZVP/COSMO)	<i>t8ewk</i>	<i>0hxtm</i>	Blind	[30, 31]
QM + LEC	DSD-BLYP-D3(BJ)/def2-TZVPD//PBEh-3c[DCOSMO-RS] + RRHO[GFN-xTB[GBSA]] + Gsolv(COSMO-RS[TZVPD]) and linear fit		<i>xvxzd</i>	Blind	[32]
QM + LEC	ReScosS conformations // DSD-BLYP-D3 reranking // COSMOtherm pKa: DSD-BLYP-D3(BJ)/def2-TZVPD// PBE-D3(BJ)/def2-TZVP/COSMO + RRHO[GFN-xTB + GBSA-water] + Gsolv[COSMO-RS(FINE17/TZVPD)] level and COSMOtherm pKa applied at the single conformer pair level (COSMOtherm17.0.5 release and BP-TZVPD-FINE-C30-1701 parameterization)	<i>eyetm</i>	<i>8xt50</i>	Blind	[32]
QM + LEC	ReScosS conformations // COSMOtherm pKa: DSD-BLYP-D3(BJ)/def2-TZVPD// PBE-D3(BJ)/def2-TZVP/COSMO + RRHO[GFN-xTB + GBSA-water] + Gsolv[COSMO-RS(FINE17/TZVPD)] level and COSMOtherm pKa was applied directly on the resulting conformer sets with at least 5% Boltzmann weights for each microspecies (COSMOtherm17.0.5 release and BP-TZVPD-FINE-C30-1701 parameterization)	<i>ccpmw</i>	<i>yqkga</i>	Blind	[32]
QM + MM	M06-2X/6-31G*(for bases) or 6-31+G*(for acids) for gas phase, solvation free energy using TI with explicit solvent and GAFF, solvation free energy of proton -265.6 kcal/mol	<i>0wfzo</i>		Blind	[33]
QM + MM	M06-2X/6-31G*(for bases) or 6-31+G*(for acids) for gas phase, solvation free energy using TI with explicit solvent and GAFF, solvation free energy of proton -271.88 kcal/mol	<i>z3btx</i>		Blind	
QM + MM	M06-2X/6-31G*(for bases) or 6-31+G*(for acids) + thermal state correction for gas phase, solvation free energy using TI with explicit solvent and GAFF, solvation free energy of proton -265.6 kcal/mol	<i>758j8</i>		Blind	
QM + MM	M06-2X/6-31G*(for bases) or 6-31+G*(for acids) + thermal state correction for gas phase, solvation free energy using TI with explicit solvent and GAFF, solvation free energy of proton -271.88 kcal/mol	<i>hgn83</i>		Blind	

* Microscopic pK_a submissions were blind, however, participant requested a correction after blind submission deadline for macroscopic pK_a submissions. Therefore, these were assigned submission IDs in the form of $nb\#\#\#$.

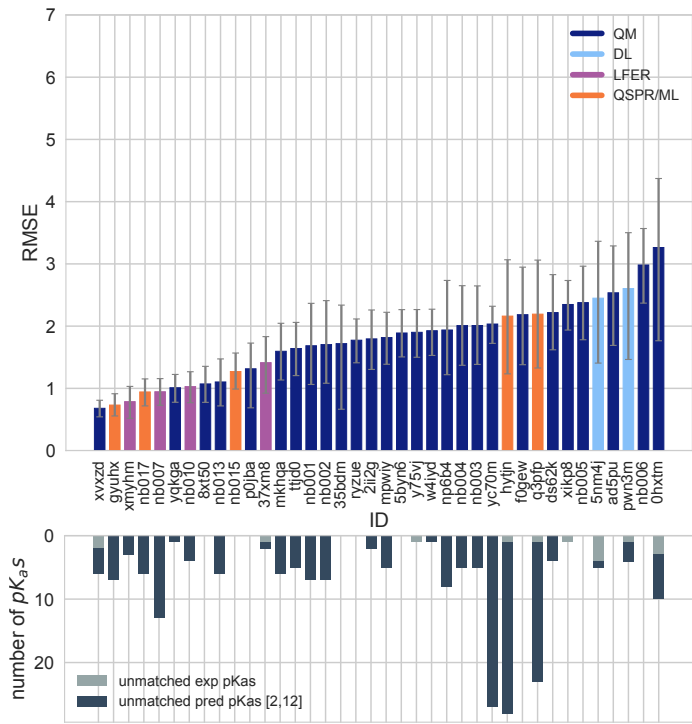


Figure 2. RMSE and unmatched pK_a counts vs. submission ID plots for macroscopic pK_a predictions based on Hungarian matching. Methods are indicated by submission IDs. RMSE is shown with error bars denoting 95% confidence intervals obtained by bootstrapping over challenge molecules. Lower bar plots show the number of unmatched experimental pK_a s (light grey, missing predictions) and the number of unmatched pK_a predictions (dark grey, extra predictions) for each method between pH 2 and 12. Submission IDs are summarized in Table 1. Submission IDs of the form $nb\#\#\#$ refer to non-blinded reference methods computed after the blind challenge submission deadline. All others refer to blind, prospective predictions. Submissions are colored by their method categories. Light blue colored database look up methods are utilized as the null prediction method.

units, MAE of 1.5 pK_a units, R^2 of 0.2 and Kendall's Tau of 0.3. Many methods were observed to have prediction performance advantage over the Null predictions shown in light blue in Fig. 2 and Fig. 3 considering all the performance metrics as a whole. In terms of correlation statistics the null methods are the worst performers, except *0hxtm*. From the perspective of accuracy-based statistics (RMSE and MAE), only the top 10 methods were observed to have significantly lower errors than the null methods considering the uncertainty of error metrics expressed as 95% confidence intervals.

Distribution of macroscopic pK_a prediction signed errors observed in each submission was plotted in Fig. 7A as ridge plots based on Hungarian matching. *2i12g*, *f0gew*, *np64b*, *p0jba*, and *yc70m* tend to overestimate and *5byn6*, *ryzue*, and *w4ydy* tend to underestimate macroscopic pK_a values.

In addition the statistics related to the value of pK_a , we have also analyzed missing or extra pK_a predictions. Analysis of the pK_a values with accuracy- and correlation-based error metrics was only possible after assignment of predicted macroscopic pK_a s to experimental pK_a s through the Hungarian matching, although, this approach masks pK_a prediction issues in the form of extra or missing macroscopic pK_a predictions. To capture this form of prediction errors we reported the number of unmatched experimental pK_a s (missing pK_a predictions) and the number of unmatched predicted pK_a s (extra pK_a predictions) after Hungarian matching for each method. Both missing and extra pK_a prediction counts were only considered for the pH range of 2-12 which was the limits of experimental measurements. The lower subplot of Fig. 2 shows the total count of unmatched experimental or predicted pK_a s for all the molecules in each prediction set. The order of submission IDs in the x-axis follows the RMSD based ranking so that the performance of each methods from both pK_a value accuracy and the number of pK_a s can be viewed together. Presence of missing or extra macroscopic pK_a predictions is a critical error, because inaccuracy in predicting the correct number of macroscopic transitions shows that methods are failing predict the correct set of charge states, i.e. failing to predict the correct number of ionization states that can be observed between the specified pH range.

In challenge results, extra macroscopic pK_a predictions were found to be more common than missing pK_a predictions. In

391 p_aK prediction evaluations usually accuracy of ionization states predicted within a pH range seen is neglected. When predictions
 392 are only evaluated for p_aK value accuracy with numerical matching algorithms more p_aK predictions are likely to lead to lower
 393 prediction errors. Therefore, it is not surprising that methods are biased to predict extra p_aK values. The SAMPL6 p_aK Challenge
 394 experimental data consists of 31 macroscopic p_aKs in total, measured for 24 molecules (6 molecules in the set have multiple
 395 p_aKs). Within the 10 methods with lowest RMSE only *xvxzd* method has an error of missing predicted p_aK (2 unmatched out
 396 of 31 experimental p_aKs), and all other methods that rank top 10 according to RMSE have extra predicted p_aKs ranging from 1
 397 to 13. Two prediction sets without any extra p_aK predictions and low RMSE are *8xt50* (ReSCoSS conformations // DSD-BLYP-D3
 398 reranking // COSMOtherm pKa) and *nb015* (ChemAxon/Chemicalize).

399 3.1.1 Consistently well performing methods for macroscopic p_aK prediction

400 Methods ranked differently when ordered by different error metrics, although there were a couple of methods that consistently
 401 ranked at the top fraction. By using a combinatorial criteria that takes all multiple statistical metrics and unmatched p_aK counts
 402 into account, we identified a short list of consistently well performing methods for macroscopic p_aK predictions, shown in Table 2.
 403 The criteria for selection was ranking in Top 10 according to RMSE, MAE, R², and Kendall's Tau and also having a combined
 404 unmatched p_aK (extra and missing p_aKs) count less than 8 (a third of the number of compounds). The resulted in a list of four
 405 methods which are consistently well performing across all criteria.

406 Consistently well performing methods for macroscopic p_aK prediction included methods from all categories. Two methods of
 407 the QM+LEC category were *xvxzd* (DSD-BLYP-D3(BJ)/def2-TZVPD//PBEh-3c[DCOSMO-RS] + RRHO(GFN-xTB[GBSA]) + Gsolv(COSMO-
 408 RS[TZVPD]) and linear fit) and *(8xt50)* (ReSCoSS conformations // DSD-BLYP-D3 reranking // COSMOtherm pKa) and both used
 409 COSMO-RS approach. Empirical p_aK predictions with top performance were both proprietary softwares. From QSPR and LFER
 410 categories, *gyuhx* (Simulation Plus) and *xmyhm* (ACD/pKa Classic) were the methods that made it to consistently well performing
 411 methods list. Simulation Plus p_aK prediction method consisted of 10 artificial neural network ensembles trained on 16,000
 412 compounds for 10 classes of ionizable atoms. Atom type and local molecular environment was how the ionization class of each
 413 atom was determined [34]. ACD/pKa Classic which was trained on method 17,000 compounds uses Hammett-type equations
 414 and tries to capture effects related to tautomeric equilibria, covalent hydration, resonance effects, and α , β -unsaturated systems
 415 [20].

Table 2. Four consistently well-performing prediction methods for macroscopic p_aK prediction based on consistent ranking within the Top 10 according to various statistical metrics. Submissions were ranked according to RMSE, MAE, R², and τ . Consistently well-performing methods were selected as the ones that rank in the Top 10 in each of these statistical metrics. These methods also have less than 2 unmatched experimental p_aKs and less than 7 unmatched predicted p_aKs according to Hungarian matching. Performance statistics are provided as mean and 95% confidence intervals.

Submission ID	Method Name	RMSE	MAE	R ²	Kendall's Tau (τ)	Unmatched Exp. p _a K Count	Unmatched Pred. p _a K Count [2,12]
<i>xvxzd</i>	Full quantum chemical calculation of free energies and fit to experimental p _a K	0.68 [0.54, 0.81]	0.58 [0.45, 0.71]	0.94 [0.88, 0.97]	0.82 [0.68, 0.92]	2	4
<i>gyuhx</i>	S+pKa	0.73 [0.55, 0.91]	0.59 [0.44, 0.74]	0.93 [0.88, 0.96]	0.88 [0.8, 0.94]	0	7
<i>xmyhm</i>	ACD/pKa Classic	0.79 [0.52, 1.03]	0.56 [0.38, 0.77]	0.92 [0.85, 0.97]	0.81 [0.68, 0.9]	0	3
<i>8xt50</i>	ReSCoSS conformations // DSD-BLYP-D3 reranking // COSMOtherm pKa	1.07 [0.78, 1.36]	0.81 [0.58, 1.07]	0.91 [0.84, 0.95]	0.80 [0.68, 0.89]	0	0

416 In Figure 4 prediction vs. experimental data correlation plots of macroscopic p_aK predictions with 4 consistently well-performing
 417 methods, a representative average method, and the null method(*5nm4j*). The representative method with average performance
 418 (*2ii2g* (EC-RISM/MP2/cc-pVTZ-P2-q-noThiols-2par)) was selected as the method with the highest RMSE below the median of all
 419 methods.

420 3.1.2 Which chemical properties are driving macroscopic p_aK prediction failures?

421 In addition to comparing the performance of methods that participated in the SAMPL6 Challenge, we also wanted to analyze
 422 macroscopic p_aK predictions from the perspective of challenge molecules and determine whether particular compounds suffer
 423 from larger inaccuracy in p_aK predictions. The goal of this analysis is to provide guidance on which molecular properties or
 424 moieties might be causing larger p_aK prediction error. In Fig. 5 2D depictions of challenge molecules are presented with MAE cal-
 425 culated for their macroscopic p_aK predictions over all methods, based on Hungarian match. For multiprotic molecules MAE was
 426 averaged over all the p_aKs. For the analysis of p_aK prediction accuracy observed for each molecule, MAE is a more appropriate

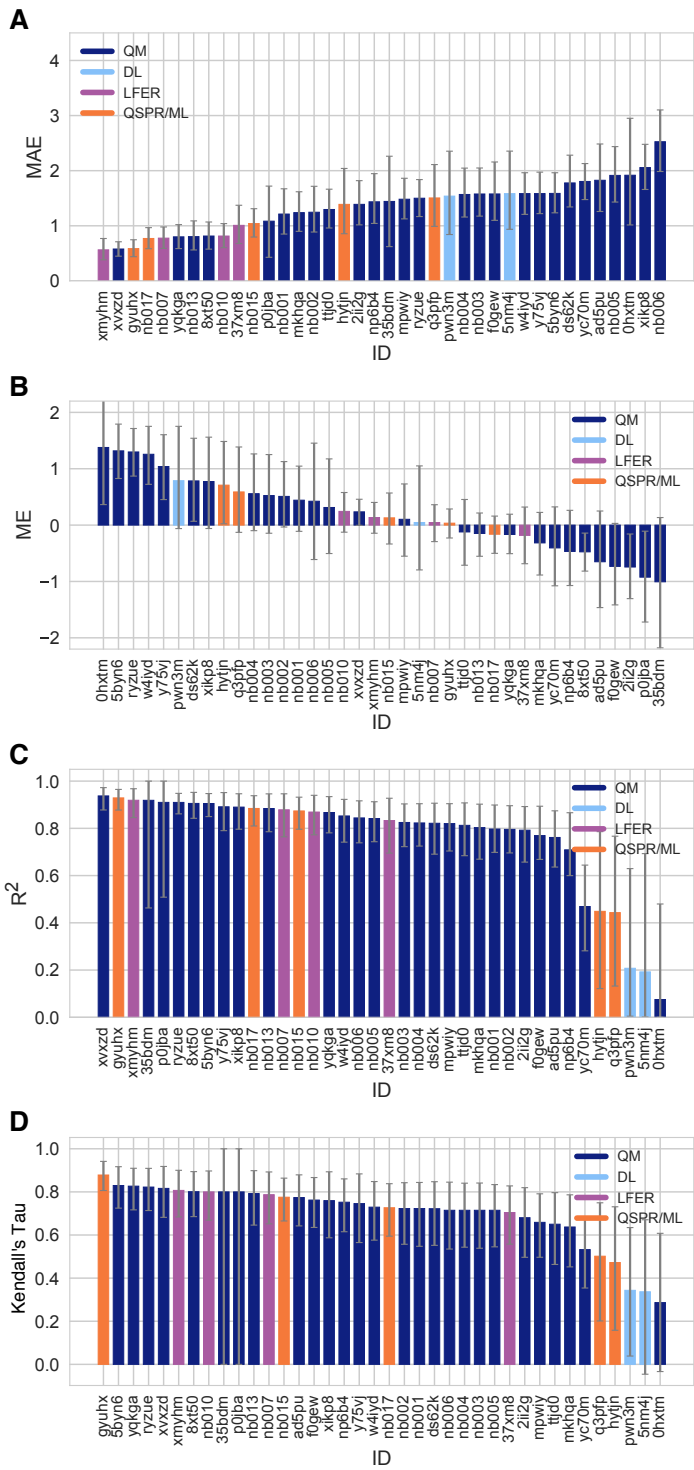


Figure 3. Additional performance statistics for macroscopic pKa predictions based on Hungarian matching. Methods are indicated by submission IDs. Mean absolute error (MAE), mean error (ME), Pearson's R², and Kendall's Rank Correlation Coefficient Tau (τ) are shown, with error bars denoting 95% confidence intervals obtained by bootstrapping over challenge molecules. Refer to Table 1 for submission IDs and method names. Submissions are colored by their method categories. Light blue colored database look up methods are utilized as the null prediction method.

statistical value than RMSE for following global trends. This is because MAE value less sensitive to outliers than is RMSE.

A comparison of prediction performance of individual molecules is shown in Fig. 6. In Fig. 6A MAE each molecule is shown

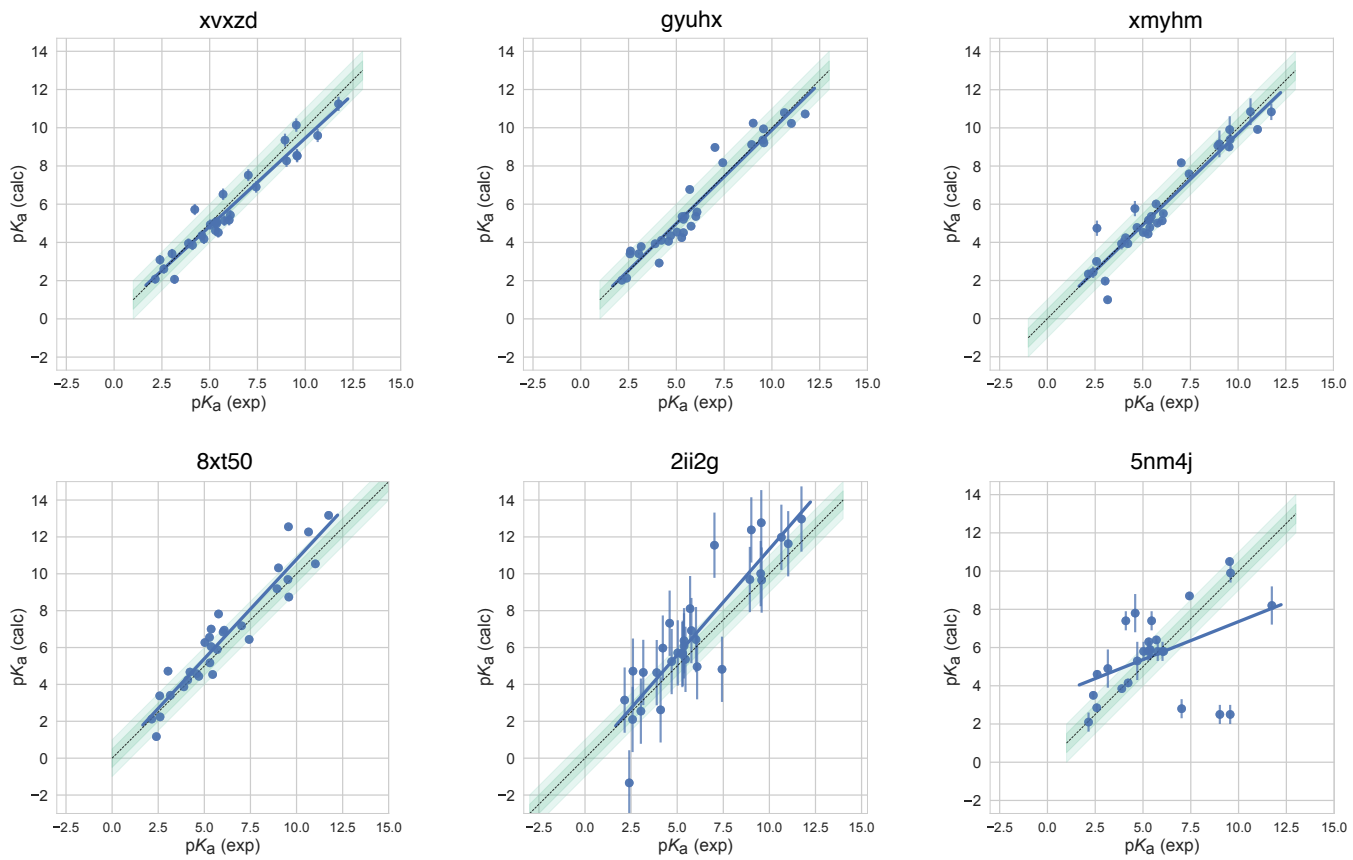


Figure 4. Predicted vs. experimental value correlation plots of 4 consistently well-performing methods, a representative method with average performance (2ii2g), and the null method (5nm4j). Dark and light green shaded areas indicate 0.5 and 1.0 units of error. Error bars indicate standard error of the mean of predicted and experimental values. Experimental p K_a SEM values are too small to be seen under the data points. EC-RISM/MP2/cc-pVTZ-P2-q-noThiols-2par method (2ii2g) was selected as the representative method with average performance because it is the method with the highest RMSE below the median.

429 considering all blind predictions and reference calculations. A cluster of molecules marked orange and red have higher than
 430 average MAE. Molecules marked red (SM06, SM21, and SM22) are the only compounds in SAMPL6 dataset with bromo or iodo
 431 groups and they suffered a macroscopic p K_a prediction error in the range of 1.7-2.0 p K_a units in terms of MAE. Molecules marked
 432 orange (SM03, SM10, SM18, SM19, and SM20) all have sulfur-containing heterocycles, and all molecules except SM18 of this
 433 group have MAE larger than 1.6 p K_a unit. SM18 despite containing thiazole group has a low MAE. SM18 is the only compound
 434 with three experimental p K_a s and we suspect presence of multiple experimental p K_a s could have a masking affect on the errors
 435 captured by MAE with Hungarian matching due to more pairing choices.

436 We analyzing MAE of each molecule for empirical(LFER and QSPR/ML) and QM-based physical methods (QM, QM+LEC, and
 437 QM+MM) separately for more insight. Fig. 6B shows that the difficulty of predicting p K_a s of the same subset of molecules was
 438 a trend conserved in the performance of physical methods. For QM-based methods too sulfur containing heterocycles, amide
 439 next to aromatic heterocycles, compounds with iodo and bromo domains have lower p K_a prediction accuracy.

440 SAMPL6 p K_a set consists of only 24 small molecules which limits our ability to do statistically confirm the determination of
 441 which chemical substructures cause greater errors in p K_a predictions. Still the trends seen in this challenge distinguish molecules
 442 with iodo, bromo, and sulfur-containing heterocycles with larger prediction errors of macroscopic p K_a value. We hope that
 443 reporting this observation will lead to improvement of methods for similar compounds with such moieties.

444 We have also looked for correlation with molecular descriptors for finding other potential explanations for why macroscopic
 445 p K_a predictions were larger in some molecules. While testing correlation between errors and many molecular descriptors it
 446 is important to keep the possibility of spurious correlations in mind. We haven't observed any significant correlation between

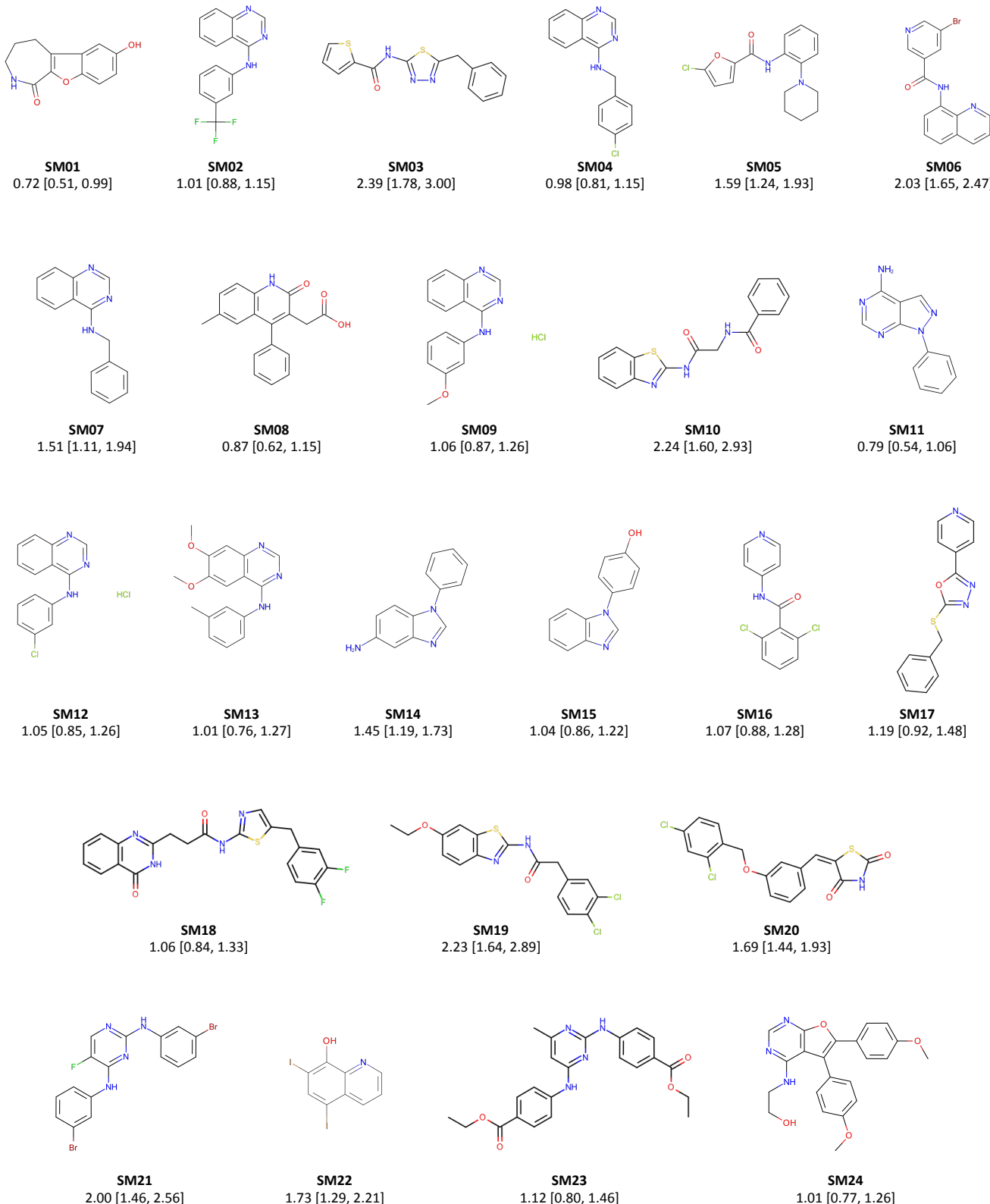
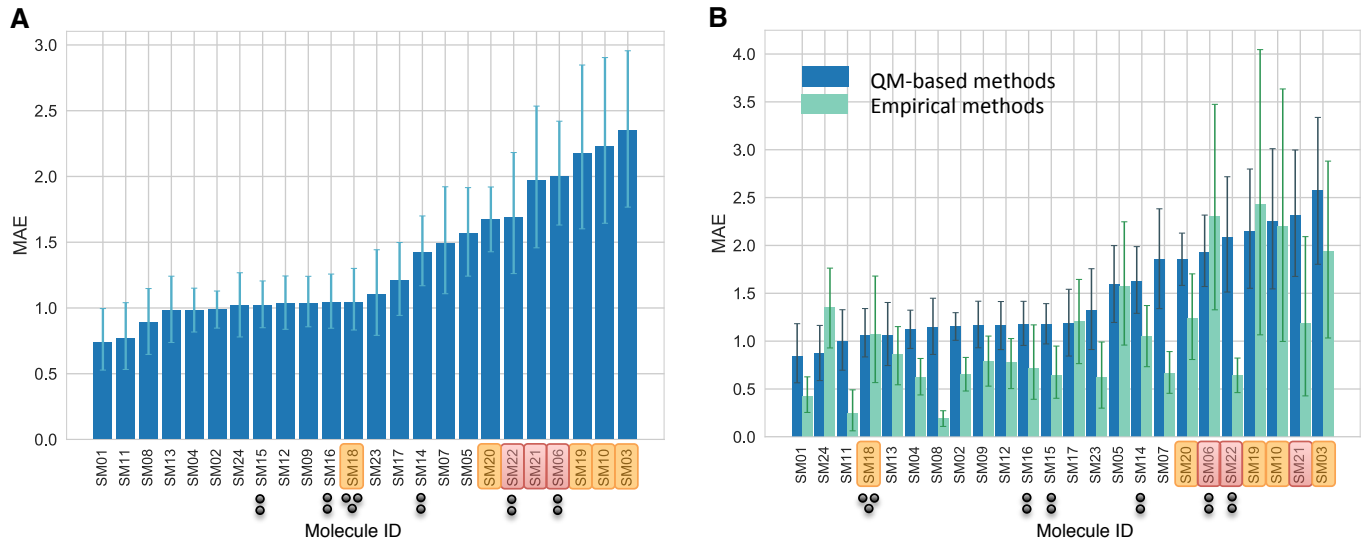
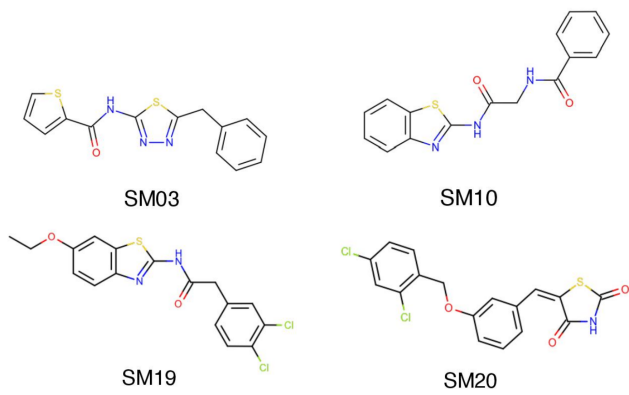


Figure 5. Molecules of SAMPL6 Challenge with MAE calculated for all macroscopic pK_a predictions. MAE calculated considering all prediction methods indicate which molecules had the lowest prediction accuracy in SAMPL6 Challenge. MAE values calculated for each molecule include all the matched pK_a values, which could be more than one per method for multiprotic molecules (SM06, SM14, SM15, SM16, SM18, SM22). Hungarian matching algorithm was employed for pairing experimental and predicted pK_a values. MAE values are reported with 95% confidence intervals.



C SAMPL6 molecules with sulfur-containing heterocycles



● 3 experimental pK_a values Sulfur-containing heterocycles
● 2 experimental pK_a values Bromo and iodo groups

D SAMPL6 molecules with bromo and iodo groups

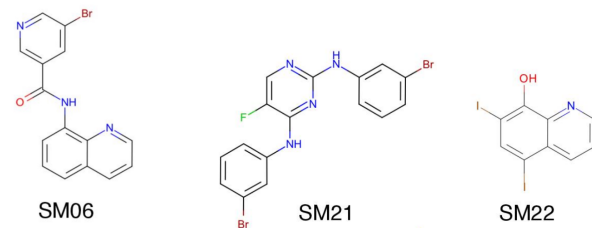


Figure 6. Average prediction accuracy calculated over all prediction methods was lower for molecules with sulfur-containing heterocycles, bromo, and iodo groups. (A) MAE calculated for each molecule as an average of all methods. (B) MAE of each molecule broken out by method category. QM-based methods (blue) include QM predictions with or without linear empirical correction. Empirical methods (green) include QSAR, ML, DL, and LFER approaches. (C) Depiction of SAMPL6 molecules with sulfur-containing heterocycles. (D) Depiction of SAMPL6 molecules with iodo and bromo groups.

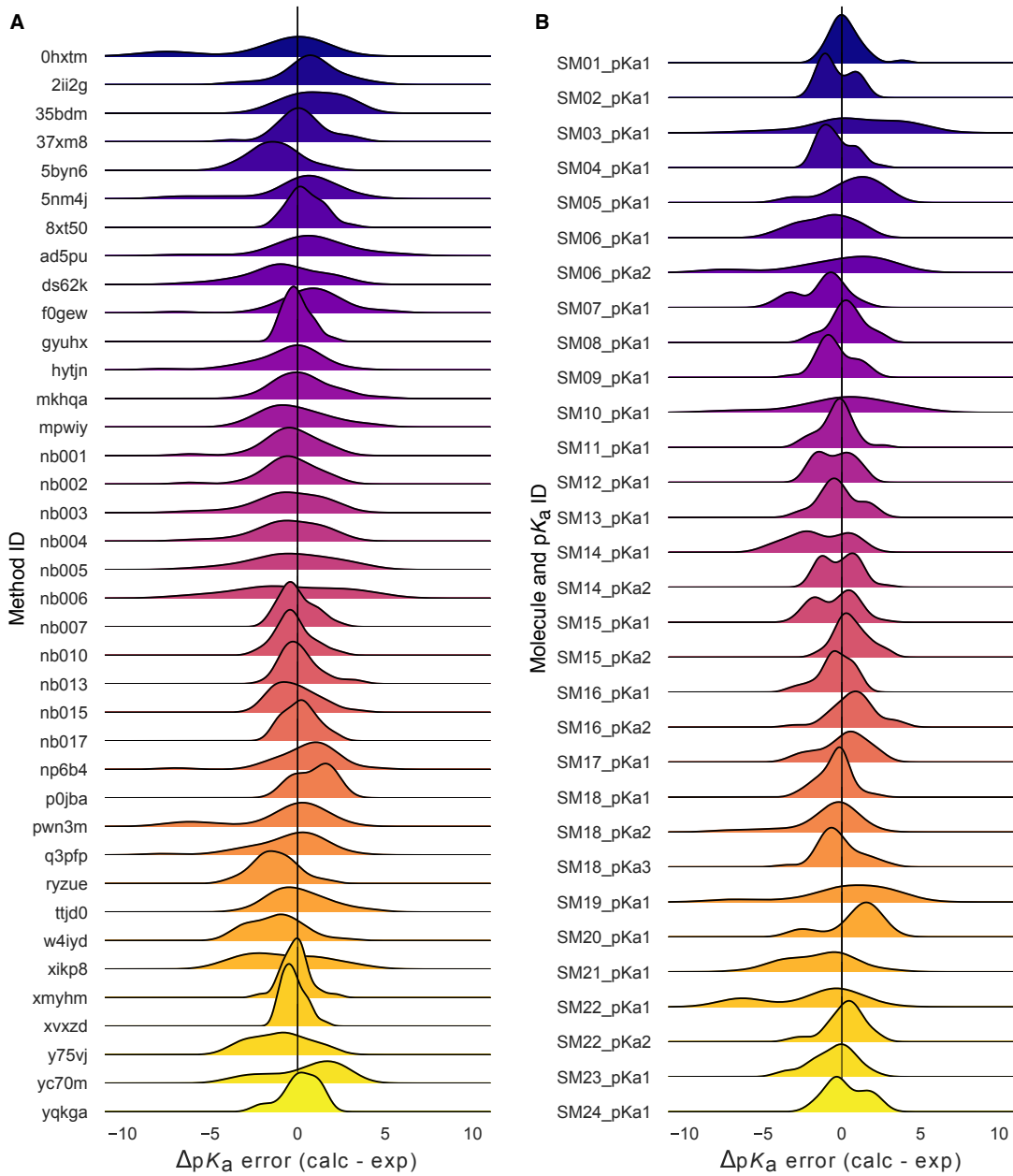


Figure 7. Macroscopic pK_a prediction error distribution plots show how prediction accuracy varies across methods and individual molecules. (A) pK_a prediction error distribution for each submission for all molecules according to Hungarian matching. (B) Error distribution for each SAMPL6 molecule for all prediction methods according to Hungarian matching. For multiprotic molecules, pK_a ID numbers (pKa1, pKa2, and pKa3) were assigned in the direction of increasing experimental pK_a value.

numerical pK_a predictions and the descriptors we have tested. First of all, higher number of experimental pK_a s (Fig. 6A) did not seem to associate with lower pK_a prediction performance. But we need to keep in mind that there was a low representation of multiprotic compounds in the SAMPL6 set (5 molecules with 2 macroscopic pK_a s and one molecule with 3 macroscopic pK_a s). Other descriptors we checked for were presence of amide groups, molecular weight, heavy atom count, rotatable bond count, heteroatom count, heteroatom to carbon ratio, ring system count, maximum ring size, and the number of microstates (as enumerated for the challenge). Correlation plots and R^2 values can be seen in Fig. S2. We had suspected that pK_a prediction methods may be trained better for moderate values (4-10) than extreme values as molecules with extreme pK_a s are less likely to change ionization states close to physiological pH. To test this we look at the distribution of absolute errors calculated for all molecules and challenge predictions binned by experimental pK_a value 2 pK_a unit increments. As can be seen in Fig. S3B, the value of true macroscopic pK_a s was not a factor affecting prediction error seen in SAMPL6 Challenge.

Fig. 7B is helpful to answer the question of "Are there molecules with consistently overestimated or underestimated pK_a s?". This ridge plots shows the error distribution of each experimental pK_a . SM02_pKa1, SM04_pKa1, SM14_pKa1, and SM21_pKa1 were underestimated by majority of the prediction methods for more than 1 pK_a unit. SM03_pKa1, SM06_pKa2, SM19_pKa1, and SM20_pKa1 were overestimated by the majority of the preodction methods for more than 1 pK_a unit. SM03_pKa1, SM06_pKa2, SM10_pKa1, SM19_pKa1, and SM22_pKa1 have the highest spread of errors and were less accurately predicted overall. Refer to Ridge plots of Delta pKa error to identify compounds that were frequently mispredicted.

3.2 Analysis of microscopic pK_a predictions using microstates determined by NMR for 8 molecules

The common approach for analysing microscopic pK_a prediction accuracy has been to compare it to experimental macroscopic pK_a data, assuming experimental pK_a s describe titrations of distinguishable sides and, therefore, equal to microscopic pK_a s. But this typical approach fails to evaluate the methods in microscopic level.

Analysis of microscopic pK_a predictions of the SAMPL6 Challenge was not straight-forward due to lack of experimental data with microscopic detail. For 24 molecules macroscopic pK_a s were determined with spectrophotometric method. For 18 molecules single macroscopic titration was observed and for 6 molecules multiple experimental pK_a s were reported. For 18 molecules with single experimental pK_a it is probabable that the molecules are monoprotic and therefore macroscopic pK_a value is equal to the microscopic pK_a , but there is no direct experimental evidence to support that this is the case but only the support from prediction methods. There is always the possibility that the macroscopic pK_a observed is the result of two different titrations overlapping closely with respect to pH. We did not want to bias the blind challenge analysis with any prediction method. Therefore, we believe analyzing the microscopic pK_a predictions via Hungarian matching to experimental values with the assumption that the 18 molecules have single titratable site is not the best approach. Instead analysis at the level of macroscopic pK_a s is much more appropriate when a numerical matching scheme is the only option to evaluate predictions using macroscopic experimental data.

For a subset of the molecules in the dataset of 8 molecules, dominant microstates were inferred from NMR experiments. This dataset was extremely useful for guiding the assignment between experimental and predicted pK_a values based on microstates. In this section we present the performance evaluations of microscopic pK_a predictions for only the 8 compounds with experimentally determined dominant microstates.

3.2.1 Microstate-based matching revealed errors masked by pK_a value-based matching between experimental and predicted pK_a s

Comparing microscopic pK_a predictions directly to macroscopic experimental pK_a values with numerical matching can lead to underestimation of errors. To demonstrate how numerical matching often masks the pK_a prediction errors we compared the performance analysis done by Hungarian matching to microstate-based matching for 8 molecules presented in Fig. 8A. RMSE calculated for microscopic pK_a predictions matched to experimental values via Hungarian matching is shown in Fig. 8B, while Fig. 8C shows RMSE calculated via microstate-based matching. What is important to notice is that the Hungarian matching leads to significantly lower RMSE compared to microstate-based matching. The reason is that the Hungarian matching assigns experimental pK_a values to predicted pK_a values only based on the closeness of the numerical values, without consideration of the relative population of microstates and microstate identities. Because of that a microscopic pK_a value that describes a transition between very low population microstates (high energy tautomers) can be assigned to the experimental pK_a if it has the closest pK_a value. This is not helpful, because in reality the microscopic pK_a s that influence the observable macroscopic pK_a the most are the ones with higher populations (transitions between low energy tautomers).

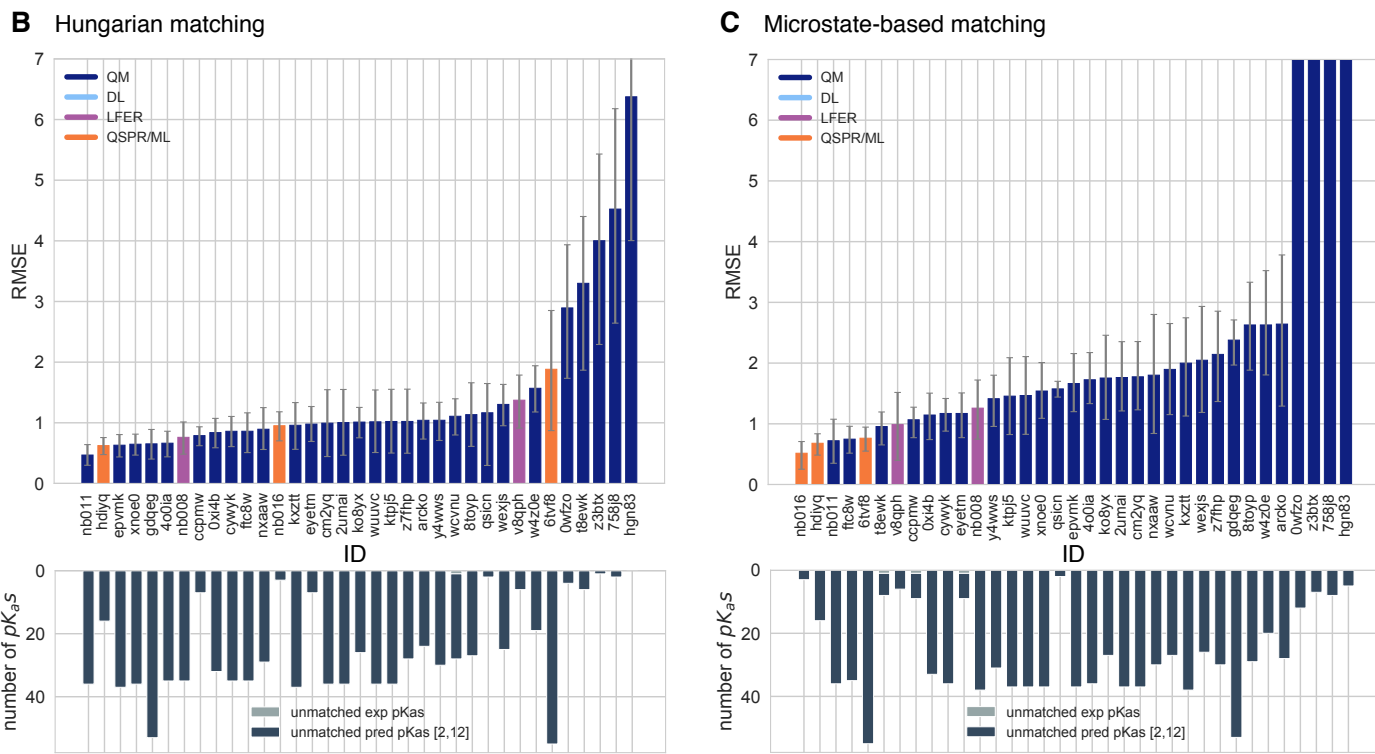
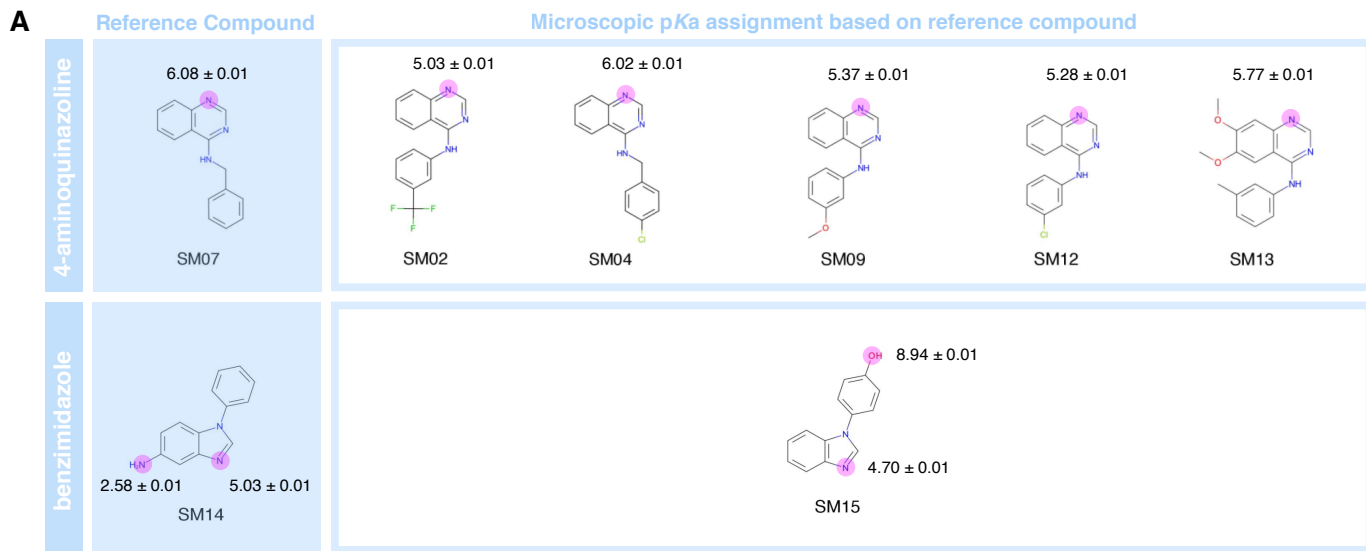


Figure 8. NMR determination of dominant microstates allowed in depth evaluation of microscopic pKa predictions of 8 compounds.

A Dominant microstate sequence of two compounds (SM07 and SM14) were determined by NMR [7]. Based on these reference compounds dominant microstates of 6 other derivative compounds were inferred and experimental pKa values were assigned to titratable groups with the assumption that only the dominant microstates have significant contributions to the experimentally observed pKa. **B** RMSE vs. submission ID and unmatched pKa vs. submission ID plots for the evaluation of microscopic pKa predictions of 8 molecules by Hungarian matching to experimental macroscopic pKas. **C** RMSE vs. submission ID and unmatched pKa vs. submission ID plots showing the evaluation of microscopic pKa predictions of 8 molecules by microstate-based matching between predicted microscopic pKas and experimental macroscopic pKa values. Submissions *0wfzo*, *z3bt8*, *758j8*, and *hgn83* have RMSE values bigger than 10 pKa units which are beyond the y-axis limits of subplot **C** and **B**. RMSE is shown with error bars denoting 95% confidence intervals obtained by bootstrapping over challenge molecules. Lower bar plots show the number of unmatched experimental pKas (light grey, missing predictions) and the number of unmatched pKa predictions (dark grey, extra predictions) for each method between pH 2 and 12. Submission IDs are summarized in Table 1.

495 The number of unmatched predicted microscopic pK_a s are shown in lower bar plots of Fig. 8B and C, to emphasize the large
496 number of microscopic pK_a predictions submitted by many methods. In the case of microscopic pK_a the number of unmatched
497 predictions do not indicate an error in the form of an extra predicted pK_a , because the spectrophotometric experiments do not
498 capture all microscopic pK_a s theoretically possible (transitions between all pairs of microstates that are 1 proton apart). pK_a s
499 of transitions to and from very high energy tautomers are very hard to measure by experimental methods, including the most
500 sensitive methods like NMR. The reason we plotted them was more to demonstrate how the increased number of prediction
501 value choices for Hungarian matching can lead to erroneously low RMSE values. We have also checked how often Hungarian
502 matching led to the correct matches between predicted and experimental pK_a in terms of the microstate pairs, i.e. how often the
503 microstate pair of the Hungarian match recapitulates the dominant microstate pair of the experiment. The overall accuracy of
504 correct microstate pair match was found to be low for SAMPL6 Challenge submission. Fig. S4 shows that for most methods the
505 predicted microstate pair selected by Hungarian match did not match experimentally determined microstate pair. This means
506 the lower RMSE results obtained from Hungarian matching are low for the wrong reason. Matching experimental and predicted
507 values on the basis of microstate IDs do not suffer from this problem.

508 The disadvantage of the evaluation through microstate-based matching approach is that the conclusions in this section are
509 only about a subset of challenge compounds with limited diversity. This subset is composed of 6 molecules 4-aminoquinazoline
510 and 2 molecules with benzimidazole scaffolds, and a total of 10 pK_a values. The sequence of dominant microstates for SM07 and
511 SM14 were determined by NMR experiments directly [7], and dominant microstates of their derivatives were inferred taking them
512 as reference (Fig. 8). Although, we believe that microstate-based evaluation is more informative, the lack of a large experimental
513 dataset limits the conclusions to a very narrow chemical diversity.

514 3.2.2 Accuracy of pK_a predictions evaluated by microstate-based matching

515 Both accuracy and correlation based statistics were calculated for predicted microscopic pK_a values after microstate-based
516 matching. RMSE, MAE, ME, R^2 , and Kendall's Tau results of each method are shown in Fig. 8C and Fig. 9. A table of the calculated
517 statistics can be found in Table S4. Due to small number of data points in this set, correlation based statistics calculated shows
518 large uncertainty and provide less utility for distinguishing better performing methods. Therefore we focused more on accuracy
519 based metrics for the analysis of microscopic pK_a s than correlation based metrics. In terms of accuracy of microscopic pK_a
520 value, all three QSPR/ML based methods (*nb016* (MoKa), *hdijyq* (Simulations Plus), *6tvf8* (OE Gaussian Process)), three QM-based
521 methods (*nb011* (Jaguar), *ftc8w* (EC-RISM/MP2/cc-pVTZ-P2-q-noThiols-2par), *t8ewk* (COSMOlogic_FINE17)), and one LFER method
522 (*v8qph* (ACD/pKa GALAS)) achieved RMSE lower than 1 pK_a unit. The same 6 methods also have the lowest MAE.

523 3.2.3 Evaluating microstate prediction accuracy of methods

524 For many computational chemistry approaches including structure based modeling of protein-ligand interactions, predicting
525 the ionization state and the exact position of protons is important to guide modeling. This is why in addition to being able to
526 predict pK_a values accurately, we need pK_a prediction methods to be able to capture microscopic protonation states accurately.
527 Even when the predicted pK_a value is very accurate, the predicted protonation site can be wrong. Therefore, we assessed if
528 methods participating the SAMPL6 pK_a Challenge were predicting correctly the sequence of dominant microstates, i.e. dominant
529 tautomers of each charge state observed between pH 2 and 12.

530 Analyze which state has lowest free energy for each charge group (The sequence of "experimentally visible states")

531 Dominant microstate prediction accuracy of microscopic pK_a prediction method are shown in Fig. 10. To extract the dominant
532 tautomers predicted for the sequence of ionization states of each method, first, relative free energy of microstates were
533 calculated at reference pH 0 [17]. Then to determine dominant microstate of each charge, we have selected the lowest energy
534 tautomer for each ionization states of the charges -1, 0, 1, and 2 (the charge range captured by NMR) experiments. Then pre-
535 dicted and experimental dominant microstates were compared for each charge to calculate the fraction of correctly predicted
536 dominant tautomers. This value is reported as the dominant microstate accuracy for all charges (Fig. 10A). Dominant microstate
537 prediction errors were present the methods participating in the SAMPL6 pK_a Challenge. 10 QM and 3 QSPR/ML methods did not
538 make any mistakes in dominant microstate predictions, although, they are expected to be making mistakes in the relative ratio
539 of tautomers (free energy difference between microstates) as reflected by pK_a value errors. While all the participating QSPR/ML
540 methods showed good performance in dominant microstate prediction, LFER and some QM methods made mistakes. Accuracy
541 of the prediction of the neutral dominant tautomers was perfect for all methods, except *qsicn* (Fig. 10B). But errors in predicting
542 the major tautomer of charge +1 was much more frequent. 22 out of 35 prediction sets made at least one error in prediction the
543 lowest energy tautomer with +1 charge. We didn't include ionization states with charges -1 and +2 in this assessment because

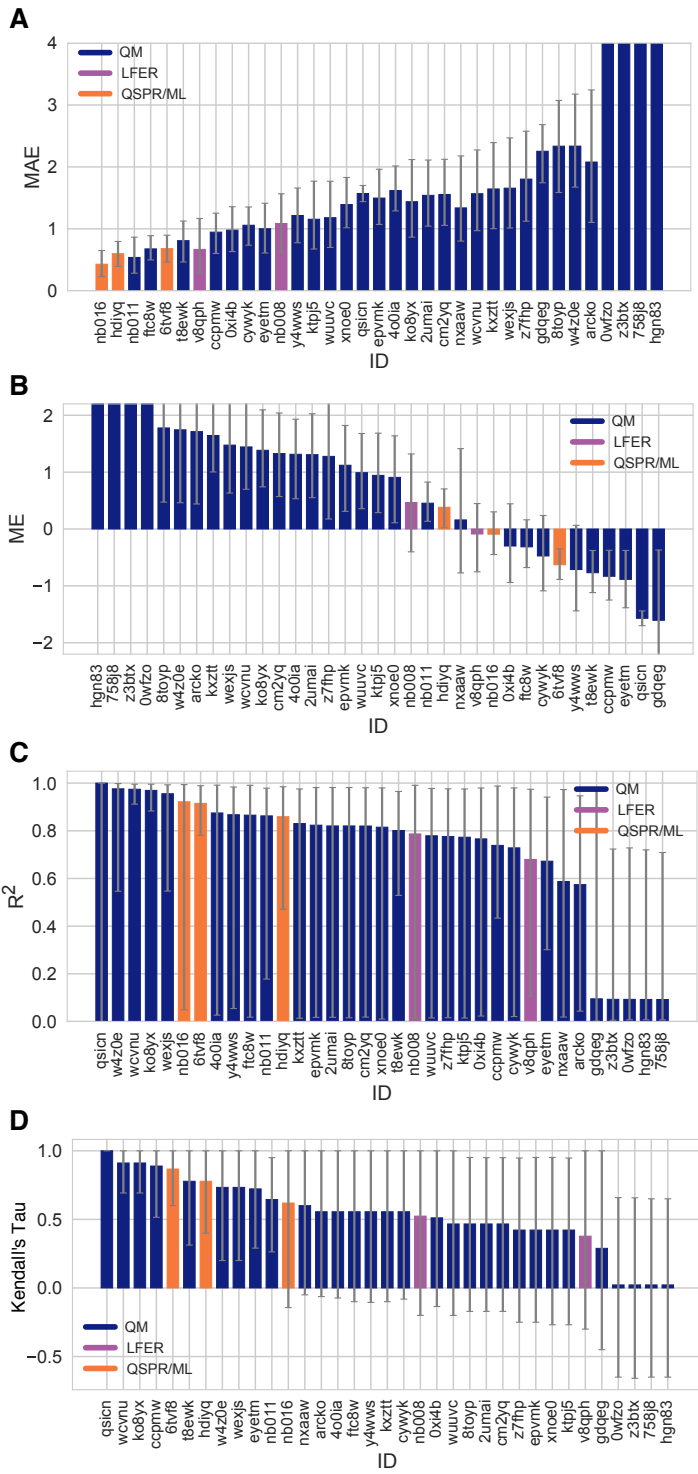


Figure 9. Additional performance statistics for microscopic pK_a predictions for 8 molecules with experimentally determined dominant microstates. Microstate-based matching was performed between experimental pK_a values and predicted microscopic pK_as. Mean absolute error (MAE), mean error (ME), Pearson's R², and Kendall's Rank Correlation Coefficient Tau (τ) are shown, with error bars denoting 95% confidence intervals obtained by bootstrapping over challenge molecules. Methods are indicated by submission IDs. Submissions are colored by their method categories. Refer to Table 1 for submission IDs and method names. Submissions 0wfzo, z3btx, 758j8, and hgn83 have MAE and ME values bigger than 10 pK_a units which are beyond the y-axis limits of subplots A and B. A large number and wide variety of methods have a statistically indistinguishable performance based on correlation based statistic (C and D), in part because of the relatively small dynamic range the small size of the set of 8 molecules.

544 we had only one compound with these charges in the dataset. Never the less, dominant tautomer prediction errors seems to
 545 be a bigger problem for charged tautomers than the neutral tautomer.

546 Experimental data of the sequence of dominant microstates was only available for 8 compounds. Therefore conclusions the
 547 performance of methods in terms of dominant tautomer prediction are limited to this narrow chemical diversity (benzimidazole and 4-aminoquinazoline derivatives). We present this analysis as a prototype of how microscopic pK_a predictions should
 548 be evaluated. To reach broad conclusions about which methods are better for capturing dominant microstates and ratios of
 549 tautomers we hope that in the future more extensive evaluations can be made with larger experimental datasets following the
 550 strategy we are demonstrating here. Even if experimental microscopic pK_a measurement data is not available, experimental
 551 dominant tautomer determinations are still informative for assessing prediction methods.

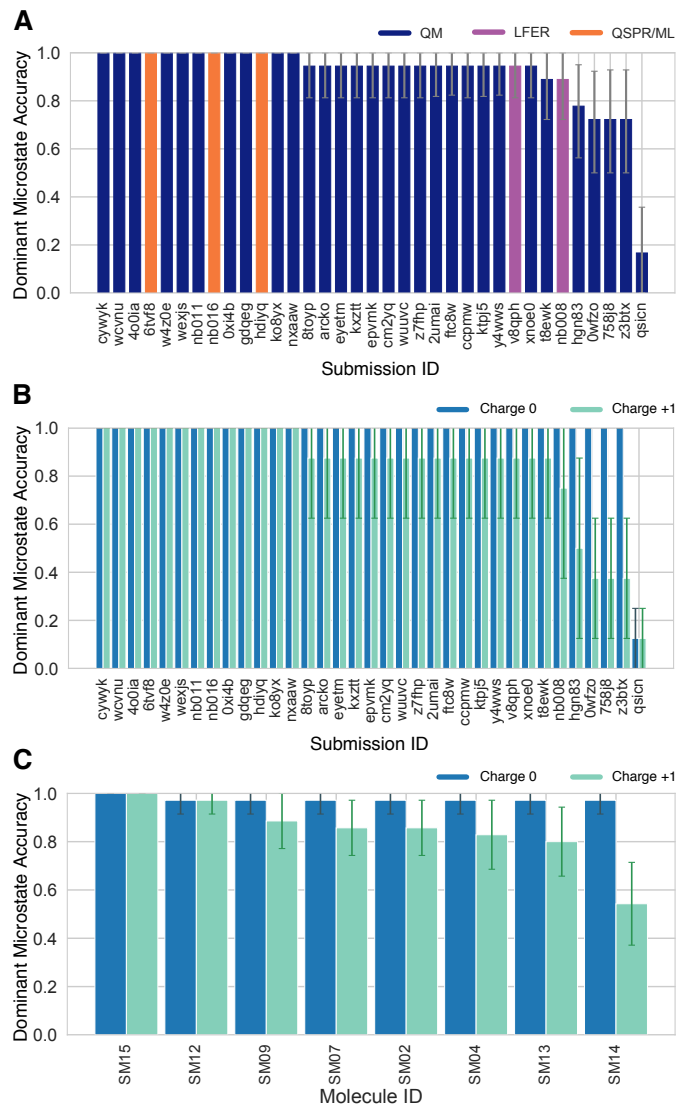


Figure 10. Some methods predicted the sequence of dominant tautomers inaccurately. Prediction accuracy of dominant microstate of each charged state was calculated using the dominant microstate sequence determined by NMR for 8 molecules as reference. **(A)** Dominant microstate accuracy vs. submission ID plot was calculated considering all the dominant microstates seen in the 8 molecule experimental microstate dataset. **(B)** Dominant microstate accuracy vs. submission ID plot was generated considering only the dominant microstates of charge 0 and +1 seen in the 8 molecule experimental microstate dataset. Accuracy of each molecule is broken out by total charge of the microstate. **(C)** Dominant microstate prediction accuracy calculated for each molecule averaged over all methods. In **(B)** and **(C)**, the accuracy of predicting the dominant neutral tautomer is showed in blue and the accuracy of predicting the dominant +1 charged tautomer is showed in green. Error bars denoting 95% confidence intervals obtained by bootstrapping.

553 Focusing on dominant microstate sequence prediction accuracy from the perspective of molecules showed that major tau-

554 tomer of SM14 cationic form was the most frequently mispredicted one. Fig. 10 shows the dominant microstate prediction
 555 accuracy calculated for individual molecules for charge states 0 and +1, averaged over all prediction methods. SM14, the
 556 molecule that exhibits highest microstate prediction error, has two experimental pK_a values that were 2.4 pK_a units apart and
 557 we suspect that could be a contributor to the difficulty of predicting microstates accurately. Other molecules are monoprotic
 558 (4-aminoquinazolines) or their experimental pK_a values are very well separated (SM14, 4.2 pK_a units). It would be very interesting
 559 to expand this assessment to a larger variety of drug-like molecules to discover for which structures tautomer predictions are
 560 more accurate and for which structure computational predictions are not as reliable.

561 3.2.4 Consistently-well performing methods for microscopic pK_a predictions

562 To determine consistently top-performing methods for microscopic pK_a predictions we have determined different criteria than
 563 macroscopic pK_a predictions: having perfect dominant microstate prediction accuracy, unmatched pK_a count of 0, and ranking
 564 in the top 10 according RMSE and MAE. Correlation based statistics were not found to have utility for discriminating perfor-
 565 mance due to large uncertainties in this statistics for a small dataset of 10 pK_a values. Unmatched predicted pK_a count was
 566 also not a consideration, since experimental data was only informative for the pK_a between dominant microstates and did not
 567 capture the all possible theoretical transitions between microstate pairs. Table 3 reports six methods that have consistent well
 568 performance according to many metrics, although evaluated only for the 8 molecule set due to limitations of the experimen-
 569 tal dataset. Six methods were divided evenly between methods of QSPR/ML category and QM category. *nb016* (MoKa), *hdiyq*
 570 (Simulations Plus), and *6tvf8* (OE Gaussian Process) were QSPR and ML based methods that performed well. *nb011* (Jaguar),
 571 *Oxi4b*(EC-RISM/B3LYP/6-311+G(d,p)-P2-phi-noThiols-2par), and *cwyk* (EC-RISM/B3LYP/6-311+G(d,p)-P2-phi-noThiols-2par) were
 572 QM predictions with linear empirical corrections with good performance with microscopic pK_a predictions.

573 Simulations Plus pK_a prediction method is the only method that appeared to be consistently well performing in both the
 574 assessment for macroscopic and microscopic pK_a prediction (and *hdiyq*). However it is worth noting that two methods that were
 575 in consistently top-performing methods list for macroscopic pK_a predictions lacked equivalent submissions of their underlying
 576 microscopic pK_a predictions and therefore could not be evaluated at the microstate level. These methods were (ACD/Classic
 577 pK_a) and *xvxzd*(DSD-BLYP-D3(B)/def2-TZVPD//PBEH-3c[DCOSMO-RS] + RRHO(GFN-xTB[GBSA]) + Gsolv(COSMO-RS[TZVPD]) and
 578 linear fit).

Table 3. Top performing methods for microscopic pK_a predictions based on consistent ranking within the Top 10 according to various statistical metrics calculated for 8 molecule dataset. Performance statistics are provided as mean and 95% confidence intervals. Submissions that rank in the Top 10 according to RMSE and MAE, and have perfect dominant microstate prediction accuracy were selected as consistently well-performing methods. Correlation-based statistics (R^2 , and Kendall's Tau), although reported in the table, were excluded from the statistics used for determining top-performing methods. This was because correlation-based statistics were not very discriminating due to narrow dynamic range and the small number of data points in the 8 molecule dataset with NMR-determined dominant microstates.

Submission ID	Method Name	Dominant Microstate Accuracy	RMSE	MAE	R^2	Kendall's Tau	Unmatched Exp. pK_a Count	Unmatched Pred. pK_a Count [2,12]
<i>nb016</i>	MoKa	1.0 [1.0, 1.0]	0.52 [0.25, 0.71]	0.43 [0.23, 0.65]	0.92 [0.05, 0.99]	0.62 [-0.14, 1.00]	0	3
<i>hdiyq</i>	S+PKa	1.0 [1.0, 1.0]	0.68 [0.49, 0.83]	0.60 [0.39, 0.80]	0.86 [0.47, 0.98]	0.78 [0.40, 1.00]	0	16
<i>nb011</i>	Jaguar	1.0 [1.0, 1.0]	0.72 [0.35, 1.07]	0.54 [0.28, 0.86]	0.86 [0.18, 0.98]	0.64 [0.26, 0.95]	0	36
<i>6tvf8</i>	OE Gaussian Process	1.0 [1.0, 1.0]	0.76 [0.55, 0.95]	0.68 [0.46, 0.90]	0.92 [0.78, 0.99]	0.87 [0.6, 1.00]	0	55
<i>Oxi4b</i>	EC-RISM/B3LYP/6-311+G(d,p)-P3NI-phi-noThiols-2par	1.0 [1.0, 1.0]	1.15 [0.75, 1.50]	0.98 [0.63, 1.36]	0.77 [0.02, 0.98]	0.51 [-0.14, 1.00]	0	33
<i>cwyk</i>	EC-RISM/B3LYP/6-311+G(d,p)-P2-phi-noThiols-2par	1.0 [1.0, 1.0]	1.17 [0.88, 1.41]	1.06 [0.74, 1.35]	0.73 [0.02, 0.98]	0.56 [-0.08, 1.00]	0	36

579 3.3 How do pK_a prediction errors impact protein-ligand binding affinity predictions?

580 Physical modeling methods for predicting protein-ligand binding affinities rely on pK_a predictions for modeling the protein and
 581 the ligand. As SAMPL6 pK_a Challenge only focused on small molecule pK_a prediction we will ignore the protonation state effects
 582 of the protein for now. Many affinity prediction methods such as docking, MM/PBSA, MM/GBSA, absolute or alchemical relative
 583 free energy calculation methods predict the affinity of a fixed protonation state of the ligand to a receptor. These models strictly
 584 depend on pK_a predictions for determining possible protonation states of the ligand in aqueous environment and in protein
 585 complex, as well as the free energy penalty to reach those states [3]. Accuracy of pK_a predictions can become a limitation for

586 the performance of physical models that try to capture molecular association.

587 In terms of the ligand protonation states, there are two ways in which the pK_a prediction errors can influence the prediction
 588 accuracy for protein-ligand binding free energies as depicted in Fig. 11. First scenario is when ligand is present in aqueous
 589 solution in multiple protonation states (Fig. 11A). When only the minor aqueous protonation state contributes to protein-ligand
 590 complex formation, overall binding free energy (ΔG_{bind}) needs to be calculated as the sum of binding affinity of the minor state
 591 and the protonation penalty of that state (ΔG_{prot}). ΔG_{prot} is a function of pH and pK_a . A 1 unit of error in pK_a value would lead to
 592 1.36 kcal/mol error in overall binding affinity, if the protonation state with the minor population binds the protein. The following
 593 equations show the calculation of overall affinity:

$$\Delta G_{bind} = \Delta G_{bind}^C + \Delta G_{prot} \quad (6)$$

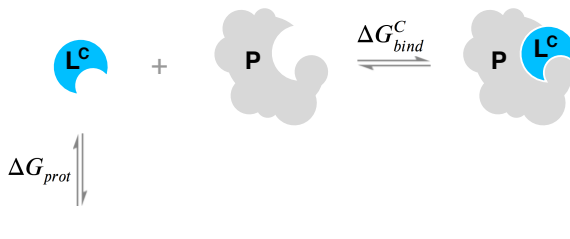
$$\Delta G_{bind} = \Delta G_{bind}^C + RT(pH - pK_a) \ln(10) \quad (7)$$

594 In addition to multiple protonation states being present in the aqueous environment, multiple charge states can contribute
 595 to complex formation (Fig. 11B). Then, overall free energy of binding needs to include a Multiple Protonation States Correction
 596 (MPSC) term (ΔG_{corr}). MPSC is a function of pH, aqueous pK_a of the ligand, and the difference between the binding free energy
 597 of charged and neutral species ($\Delta G_{bind}^C - \Delta G_{bind}^N$) as shown below:

$$\Delta G_{bind} = \Delta G_{bind}^N + \Delta G_{corr} \quad (8)$$

$$\Delta G_{bind} = \Delta G_{bind}^N - RT \ln \frac{1 + e^{-\frac{\Delta G_{bind}^C - \Delta G_{bind}^N}{RT}} 10^{pK_a - pH}}{1 + 10^{pK_a - pH}} \quad (9)$$

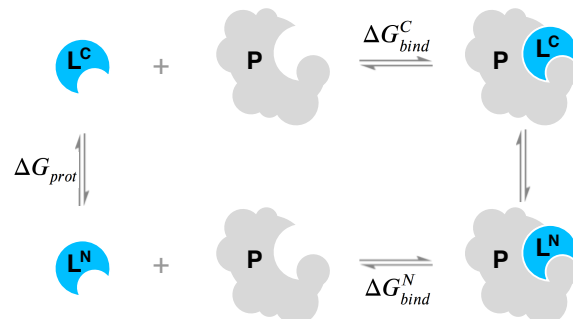
A When only the minor protonation state can bind to the protein



$$\Delta G_{bind} = \Delta G_{bind}^C + \Delta G_{prot}$$

$$\Delta G_{bind} = \Delta G_{bind}^C + RT(pH - pK_a) \ln(10)$$

B When multiple protonation states can bind to the protein



$$\Delta G_{bind} = \Delta G_{bind}^N + \Delta G_{corr}$$

$$\Delta G_{bind} = \Delta G_{bind}^N - RT \ln \frac{1 + e^{-\frac{\Delta G_{bind}^C - \Delta G_{bind}^N}{RT}} 10^{pK_a - pH}}{1 + 10^{pK_a - pH}}$$

Figure 11. Aqueous pK_a of the ligand can influence overall protein-ligand binding affinity. **A** When only the minor aqueous protonation state contributes to protein-ligand complex formation, overall binding free energy (ΔG_{bind}) needs to be calculated as the sum of binding affinity of the minor state and the protonation penalty of that state. **B** When multiple charge states contribute to complex formation, overall free energy of binding includes a multiple protonation states correction (MPSC) term (ΔG_{corr}). MPSC is a function of pH, aqueous pK_a of the ligand, and the difference between the binding free energy of charged and neutral species ($\Delta G_{bind}^C - \Delta G_{bind}^N$).

598 Using Equation 9 we can model the true MPSC (ΔG_{corr}) value with respect to the difference between pH and the pK_a of the
 599 ligand, to see when this value has significant impact to overall binding free energy. In Fig. 12, true MPSC value that needs
 600 to be added to the ΔG_{bind}^N is shown for ligands with varying binding affinity difference between protonation states ($\Delta \Delta G =$
 601 $\Delta G_{bind}^C - \Delta G_{bind}^N$) and varying free energy of binding difference between the protonation states. Fig. 12A shows the simulation of
 602 a case where for a monoprotic base which has a charged state with lower affinity than the neutral state. Solid lines show the
 603 correction. In situations where pK_a is lower than pH, correction factor disappears as the ligand fully populates the neutral

state ($\Delta G_{bind} = \Delta G_{bind}^N$). As the pK_a value gets larger than the pH, the charged state is populated more and ΔG_{corr} value increases to approach significant $\Delta\Delta G$. What is interesting to note is the pH- pK_a range that ΔG_{corr} changes. It is often assumed that for a basic ligand if pK_a of a ligand is more than 2 units higher than the pH, then only 1% of the population is in neutral state and it is safe to approximate the overall binding affinity with ΔG_{bind}^C only. Based on the relative free energy difference between ligand this assumption is not always correct. As seen in Fig. 12A, responsive region of ΔG_{corr} can span 3 pH units for a system with $\Delta\Delta G = 1\text{kcal/mol}$ or 5 pH units for a system with $\Delta\Delta G = 4\text{kcal/mol}$. This highlights that the range of pK_a values that impact binding affinity predictions is wider than previously appreciated. Molecules with pK_a s several units away from the physiological pH can still impact the overall binding affinity significantly due to MPSC.

Despite the need to capture the contributions of multiple protonations states by including MPSC in binding affinity calculations, inaccurate pK_a predictions can lead to errors in ΔG_{corr} and overall free energy of binding prediction. In Fig. 12A dashed lines show predicted ΔG_{corr} based on pK_a error of -1 units. We have chosen a pK_a error of 1 units as this is the average performance expected from the pK_a prediction methods based on the SAMPL6 Challenge. Underestimated pK_a causes underestimated ΔG_{corr} and overestimated affinities for a varying range of pH - pK_a values depending on binding affinity difference between protonation states($\Delta\Delta G$). In Fig. 12B dashed lines shows how the magnitude of the absolute error caused by calculating ΔG_{corr} with an inaccurate pK_a varies with respect to pH. Different colored lines show simulated results with varying binding affinity difference between protonation states. For a system whose charged state has lower affinity than the neutral state ($\Delta\Delta G = 2\text{kcal/mol}$), the absolute error caused by underestimated pK_a by 1 units only can be up to 0.9 kcal/mol. For a system whose charged state has even lower affinity than the neutral state ($\Delta\Delta G = 4\text{kcal/mol}$), the absolute error caused by underestimated pK_a by 1 units only can be up to 1.2 kcal/mol. The magnitude of errors contributing to overall binding affinity are too large to be neglected. Improving the accuracy of small molecule pK_a prediction methods can help to minimize the error in predicted MPSC.

With the current level of pK_a prediction accuracy as observed in SAMPL6 Challenge, is it advantageous to include MPSC in affinity predictions that may be include errors caused by pK_a predictions? We provide a comparison of the two choices to answer this question: (1) Neglecting MPSC completely and assuming overall binding affinity is captured by ΔG_{bind}^N , (2) including MPSC with potential error in overall affinity calculation. The magnitude of error caused by Choice 1 (ignoring MPSC) is depicted as solid line in Fig. 12B and the magnitude of error caused by MPSC computed with inaccurate pK_a is depicted as dashed lines. What is the best strategy? Error due to choice 1 is always larger than error due to choice 2 for all pH- pK_a values. In this scenario including MPSC improves overall binding affinity prediction. The error caused my inaccurate pK_a is smaller than the error caused by neglecting MPSC.

The same question about whether or not an MPSC calculated based on an inaccurate pK_a should be included in binding affinity predictions can be asked for different circumstances underestimated or overestimated pK_a values, charged states with higher or lower affinities than the neutral states. We tried to capture these 4 circumstances in four quadrants of Fig. 12. In the case of overestimated pK_a values (Fig. 12E-H) it can be seen that for the most of the pH- pK_a range it is more advantageous to include the predicted MPSC in affinity calculations, except a smaller window where the opposite choice would be more advantageous. For instance, for the system with $\Delta\Delta G = 2\text{kcal/mol}$ and overestimated pK_a (Fig. 12E) for the pH- pK_a region between -0.5 and 2, including predicted ΔG_{corr} causes more error than ignoring MPSC.

In reality we do not know the exact magnitude or the direction of the error of our predicted pK_a , therefore using simulated MPSC error plots to make the decision about when to include MPSC in binding affinity predictions is not possible. But based on the analysis of extreme cases, with 1 unit of pK_a error including MPSC correction is more often than not helpful in imporving binding affinity predictions. The detrimental effect of pK_a inaccuracy is still significant, however, future improvements in pK_a prediction methods can improve the accuracy of MPSC and binding affinity predictions of ligands which have multiple protonation states that contribute to aqueous or complex populations. Achieving pK_a value prediction accuracy of 0.5 units would significantly help the binding affinity models to incorporate more accurate MPSC terms.

3.4 Lessons learned from SAMPL6 pKa Challenge

Do any methods predict within experimental accuracy (how is the field doing overall)?

Common challenging factors for accurate pKa predictions. Tautomers, Heterocycles etc.

Overall results: Do any methods predict within experimental accuracy (how is the field doing overall)? Common challenging factors for accurate pKa predictions. Tautomers, Heterocycles etc.

Discussion of matching problem betwene experimental and predicted values. Difficulty of assessing predicted pKas using experimental data: matching problem Explain rationale behind how we analyze the data and determine success/failure.

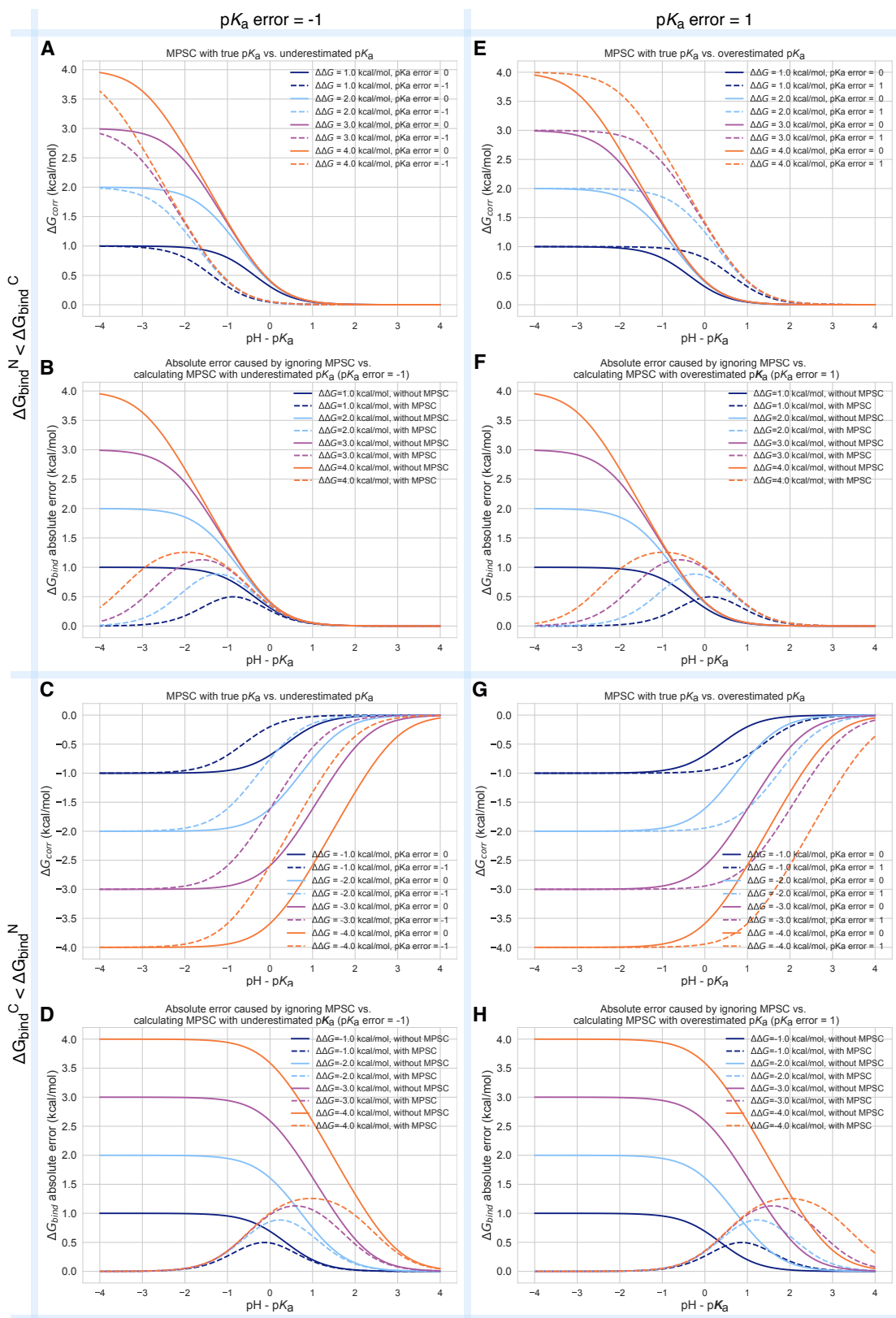


Figure 12. Inaccuracy of pK_a prediction (± 1 unit) affects the accuracy of MPSC and overall protein-ligand binding free energy calculation in varying amounts based on aqueous pK_a value and relative binding affinity of individual protonation states ($\Delta\Delta G = \Delta G_{bind}^C - \Delta G_{bind}^N$). All calculations are made for 25°C, and for a ligand with single basic titratable group. **A, C, E, and G show MPSC (ΔG_{corr}) calculated with true vs. inaccurate pK_a . **B, D, F, and H** show comparison of the absolute error to ΔG_{bind} caused by ignoring the MPSC completely (solid lines) vs. calculating MPSC based in inaccurate pK_a value (dashed lines). These plots provide guidance on when it is beneficial to include MPSC correction based on pK_a error, $pH - pK_a$, and $\Delta\Delta G$.**

653 Conclusion about prediction performance of individual molecules: SAMPL6 pKa set consisted of only 24 small molecules
654 which limits our ability to do statistical analysis to determine which chemical substructures contribute to greater errors in pKa
655 predictions. Which chemical structures make pKa predictions more difficult?

656 What can we learn from failures? Which physical effects are driving failures? Cycle closure errors

657 Factors to consider when deciding which pKa prediction method to consider? -license -how expensive is the calculation -
658 macroscopic pKa value accuracy -macrostate number accuracy -microscopic pKa value accuracy - microstate accuracy - tautomer
659 ratio, correct relative free energy between tautomers

660 Errors computed by microstate-based matching are larger compared to numerical matching algorithms. Microscopic pKa
661 analysis with numerical matching algorithms may mask errors due to higher number of guesses made.

662 Due to the size of the experimental datasets evaluation of macroscopic pK_a prediction carried more weight in assessing
663 performance of computational predictions, although microscopic pK_a evaluation can provide much more in depth analysis and
664 can be more informative about capturing reasons for failure.

665 3.5 Suggestions for future challenges

666 In the SAMPL6 pK_a Challenge there wasn't a requirement that prediction sets should report predictions for all compounds.
667 Some participants reported predictions for only a subset of compounds which may lead these methods to look more accurate
668 than others, due to missing predictions. It would have been a better choice to require submissions for whole sets for better
669 comparison of method performance.

670 **Discuss what can be done to further improve future challenges**

671 How can we maximize what we learn? What should we have people predict? How should we select compounds / measure
672 pKas?

673 **Suggestions about challenge construction**

674 Future challenge direction Challenge path: predict pKas, give people pKas to predict logDs on same molecules, then predict
675 for new set of compounds logDs without provided pKas.

676 Enumeration of protonation states before predictions (which states does one need to consider?)

677 **Suggestions about challenge analysis**

678 NMR experimental techniques could be used to validate microstate information in future challenges

679 Reporting microscopic pKa predictions with charges, microstate free energies is better Experimental dataset with microstate
680 information is more helpful.

681 What can be done to further improve future challenges How can we maximize what we learn? What should we have people
682 predict? How should we select compounds / measure pKas? NMR experimental techniques could be used to validate microstate
683 information in future challenges

684 Suggestions about challenge construction Enumeration of protonation states before predictions (which states does one need
685 to consider?) Suggestions about challenge analysis

686 Submitting pKa predictions in terms of relative free energy of microstates, from which both microscopic and macroscopic
687 pKas and fractional populations of states at and pH can be calculated. Explicit hydrogen mol2 format can be used to capture
688 individual tautomers

689 4 Conclusion

690 5 Code and data availability

- 691 • SAMPL6 pK_a challenge instructions, submissions, experimental data and analysis is available at
<https://github.com/samplchallenges/SAMPL6>

692 6 Overview of supplementary information

693 Contents of the Supplementary Information:

- 694 • TABLE S1: SMILES and InChI identifiers of SAMPL6 pK_a Challenge molecules.
695 • TABLE S2: Evaluation statistics calculated for all macroscopic pK_a prediction submissions based on Hungarian match for
696 24 molecules.

- TABLE S3: Evaluation statistics calculated for all microscopic pK_a prediction submissions based on Hungarian match for 8 molecules with NMR data.
- TABLE S4: Evaluation statistics calculated for all microscopic pK_a prediction submissions based on microstate match for 8 molecules with NMR data.
- FIGURE S1: Dominant microstates of 8 molecules were determined based on NMR measurements.
- FIGURE S2: MAE of macroscopic pK_a predictions of each molecule did not show any significant correlation with any molecular descriptor.
- FIGURE S3: The value of macroscopic pK_a was not a factor affecting prediction error seen in SAMPL6 Challenge according to the analysis with Hungarian matching.
- FIGURE S4: There was low agreement between experimental dominant microstate pairs and the predicted microstate pairs selected by Hungarian algorithm for microscopic pK_a predictions.

Extra files included in *SAMPL6-supplementary-documents.tar.gz*:

- SAMPL6-pKa-chemical-identifiers-table.csv
- macroscopic-pKa-statistics-24mol-hungarian-match.csv
- microscopic-pKa-statistics-8mol-hungarian-match-table.csv
- microscopic-pKa-statistics-8mol-microstate-match-table.csv
- experimental-microstates-of-8mol-based-on-NMR.csv
- enumerate-microstates-with-Epik-and-OpenEye-QUACPAC.ipynb
- molecule_ID_and_SMILES.csv

7 Author Contributions

Conceptualization, MI, JDC, CB, DLM ; Methodology, MI, JDC ; Software, MI, AR, ASR ; Formal Analysis, MI, ASR, AR ; Investigation, MI ; Resources, JDC; Data Curation, MI ; Writing-Original Draft, MI, JDC; Writing - Review and Editing, MI, ASR, AR, CB, DLM, JDC; Visualization, MI, AR ; Supervision, JDC, DLM, CB, ASR ; Project Administration, MI ; Funding Acquisition, JDC, DLM.

8 Acknowledgments

Complete acknowledgments section. Caitlin Bannan for guidance on working microstate definition for the challenge, Thomas Fox for MoKa reference calculations, Kiril Lanevskij for hungarian algorithm

MI, ASR, and JDC acknowledge support from the Sloan Kettering Institute. JDC acknowledges support from NIH grant P30 CA008748. MI acknowledges Doris J. Hutchinson Fellowship. We thank Brad Sherborne for his valuable insights at the conception of the pK_a challenge and connecting us with Timothy Rhodes and Dorothy Levorse who were able to provide resources and expertise for experimental measurements performed at MRL. We acknowledge Paul Czodrowski who provided feedback on multiple stages of this work: challenge construction, purchasable compound selection and manuscript. MI, ASR, AR and JDC are grateful to OpenEye Scientific for providing a free academic software license for use in this work.

Mike Chui

9 Disclosures

JDC is a member of the Scientific Advisory Board for Schrödinger, LLC. DLM is a member of the Scientific Advisory Board of OpenEye Scientific Software.

Table ref: [19, 20, 22, 23, 25] trial: [], +, -, *, #, \m

References

- [1] Manallack DT, Prankerd RJ, Yuriev E, Oprea TI, Chalmers DK. The Significance of Acid/Base Properties in Drug Discovery. *Chem Soc Rev.* 2013; 42(2):485–496. doi: [10.1039/C2CS35348B](https://doi.org/10.1039/C2CS35348B).
- [2] Manallack DT, Prankerd RJ, Nassta GC, Ursu O, Oprea TI, Chalmers DK. A Chemogenomic Analysis of Ionization Constants-Implications for Drug Discovery. *ChemMedChem.* 2013 Feb; 8(2):242–255. doi: [10.1002/cmdc.201200507](https://doi.org/10.1002/cmdc.201200507).
- [3] de Oliveira C, Yu HS, Chen W, Abel R, Wang L. Rigorous Free Energy Perturbation Approach to Estimating Relative Binding Affinities between Ligands with Multiple Protonation and Tautomeric States. *Journal of Chemical Theory and Computation.* 2019 Jan; 15(1):424–435. doi: [10.1021/acs.jctc.8b00826](https://doi.org/10.1021/acs.jctc.8b00826).

- 741 [4] **Darvey IG.** The Assignment of pKa Values to Functional Groups in Amino Acids. *Biochemical Education*. 1995 Apr; 23(2):80–82. doi: [10.1016/0307-4412\(94\)00150-N](https://doi.org/10.1016/0307-4412(94)00150-N).
- 743 [5] **Bodner GM.** Assigning the pKa's of Polyprotic Acids. *Journal of Chemical Education*. 1986 Mar; 63(3):246. doi: [10.1021/ed063p246](https://doi.org/10.1021/ed063p246).
- 744 [6] **Murray R.** Microscopic Equilibria. *Analytical Chemistry*,. 1995 Aug; p. 1.
- 745 [7] **Işık M**, Levorse D, Rustenburg AS, Ndukwe IE, Wang H, Wang X, Reibarkh M, Martin GE, Makarov AA, Mobley DL, Rhodes T, Chodera JD. pKa Measurements for the SAMPL6 Prediction Challenge for a Set of Kinase Inhibitor-like Fragments. *Journal of Computer-Aided Molecular Design*. 2018 Oct; 32(10):1117–1138. doi: [10.1007/s10822-018-0168-0](https://doi.org/10.1007/s10822-018-0168-0).
- 748 [8] **Pickard FC**, König G, Tofoleanu F, Lee J, Simmonett AC, Shao Y, Ponder JW, Brooks BR. Blind Prediction of Distribution in the SAMPL5 Challenge with QM Based Protomer and pK a Corrections. *Journal of Computer-Aided Molecular Design*. 2016 Nov; 30(11):1087–1100. doi: [10.1007/s10822-016-9955-7](https://doi.org/10.1007/s10822-016-9955-7).
- 751 [9] **Bannan CC**, Mobley DL, Skillman AG. SAMPL6 Challenge Results from \$\$pK_a\$\$ Predictions Based on a General Gaussian Process Model. *Journal of Computer-Aided Molecular Design*. 2018 Oct; 32(10):1165–1177. doi: [10.1007/s10822-018-0169-z](https://doi.org/10.1007/s10822-018-0169-z).
- 753 [10] **Işık M**, Levorse D, Mobley DL, Rhodes T, Chodera JD. Octanol–Water Partition Coefficient Measurements for the SAMPL6 Blind Prediction Challenge. *Journal of Computer-Aided Molecular Design*. 2020 Apr; 34(4):405–420. doi: [10.1007/s10822-019-00271-3](https://doi.org/10.1007/s10822-019-00271-3).
- 755 [11] **Işık M**, Bergazin TD, Fox T, Rizzi A, Chodera JD, Mobley DL. Assessing the Accuracy of Octanol–Water Partition Coefficient Predictions in the SAMPL6 Part II Log P Challenge. *Journal of Computer-Aided Molecular Design*. 2020 Apr; 34(4):335–370. doi: [10.1007/s10822-020-00295-0](https://doi.org/10.1007/s10822-020-00295-0).
- 757 [12] Special Issue: SAMPL6 (Statistical Assessment of the Modeling of Proteins and Ligands); October 2018. Volume 32, Issue 10. *Journal of Computer-Aided Molecular Design*.
- 759 [13] **Fraczkiewicz R.** In Silico Prediction of Ionization. In: *Reference Module in Chemistry, Molecular Sciences and Chemical Engineering* Elsevier; 2013. doi: [10.1016/B978-0-12-409547-2.02610-X](https://doi.org/10.1016/B978-0-12-409547-2.02610-X).
- 761 [14] **Kuhn HW.** The Hungarian Method for the Assignment Problem. *Naval Research Logistics Quarterly*. 1955 Mar; 2(1-2):83–97. doi: [10.1002/nav.3800020109](https://doi.org/10.1002/nav.3800020109).
- 763 [15] **Munkres J.** Algorithms for the Assignment and Transportation Problems. *J SIAM*. 1957 Mar; 5(1):32–28.
- 764 [16] SciPy v1.3.1, Linear Sum Assignment Documentation; Sep 27, 2019. The SciPy community. https://docs.scipy.org/doc/scipy-1.3.1/reference/generated/scipy.optimize.linear_sum_assignment.html.
- 766 [17] **Gunner MR**, Murakami T, Rustenburg AS, Işık M, Chodera JD. Standard State Free Energies, Not pKas, Are Ideal for Describing Small Molecule Protonation and Tautomeric States. *Journal of Computer-Aided Molecular Design*. 2020 May; 34(5):561–573. doi: [10.1007/s10822-020-00280-7](https://doi.org/10.1007/s10822-020-00280-7).
- 769 [18] OpenEye pKa Prospector;. OpenEye Scientific Software, Santa Fe, NM. Accessed on Jan 23, 2018. <https://www.eyesopen.com/pka-prospector>.
- 770 [19] ACD/pKa GALAS (ACD/Percepta Kernel v1.6);. Advanced Chemistry Development, Inc., Toronto, ON, Canada, 2018. <https://www.acdlabs.com/products/percepta/predictors/pKa/>.
- 772 [20] ACD/pKa Classic (ACD/Percepta Kernel v1.6);. Advanced Chemistry Development, Inc., Toronto, ON, Canada, 2018. <https://www.acdlabs.com/products/percepta/predictors/pKa/>.
- 774 [21] **Shelley JC**, Cholleti A, Frye LL, Greenwood JR, Timlin MR, Uchimaya M. Epik: A Software Program for pK a Prediction and Protonation State Generation for Drug-like Molecules. *Journal of Computer-Aided Molecular Design*. 2007 Dec; 21(12):681–691. doi: [10.1007/s10822-007-9133-z](https://doi.org/10.1007/s10822-007-9133-z).
- 777 [22] Simulations Plus ADMET Predictor v8.5;. Simulations Plus, Lancaster, CA, 2018. <https://www.simulations-plus.com/software/admetpredictor/physicochemical-biopharmaceutical/>.
- 779 [23] Chemicalize v18.23 (ChemAxon MarvinSketch v18.23);. ChemAxon, Budapest, Hungary, 2018. <https://docs.chemaxon.com/display/docs/pKa+Plugin>.
- 781 [24] **Milletti F**, Storchi L, Sforza G, Cruciani G. New and Original p K a Prediction Method Using Grid Molecular Interaction Fields. *Journal of Chemical Information and Modeling*. 2007 Nov; 47(6):2172–2181. doi: [10.1021/ci700018y](https://doi.org/10.1021/ci700018y).
- 783 [25] MoKa;. Molecular Discovery, Hertfordshire, UK, 2018. <https://www.moldiscovery.com/software/moka/>.
- 784 [26] **Zeng Q**, Jones MR, Brooks BR. Absolute and Relative pKa Predictions via a DFT Approach Applied to the SAMPL6 Blind Challenge. *Journal of Computer-Aided Molecular Design*. 2018 Oct; 32(10):1179–1189. doi: [10.1007/s10822-018-0150-x](https://doi.org/10.1007/s10822-018-0150-x).

- 786 [27] Bochevarov AD, Harder E, Hughes TF, Greenwood JR, Braden DA, Philipp DM, Rinaldo D, Halls MD, Zhang J, Friesner RA. Jaguar: A High-
787 Performance Quantum Chemistry Software Program with Strengths in Life and Materials Sciences. International Journal of Quantum
788 Chemistry. 2013 Sep; 113(18):2110–2142. doi: [10.1002/qua.24481](https://doi.org/10.1002/qua.24481).
- 789 [28] Selwa E, Kenney IM, Beckstein O, Iorga BI. SAMPL6: Calculation of Macroscopic pKa Values from Ab Initio Quantum Mechanical Free
790 Energies. Journal of Computer-Aided Molecular Design. 2018 Oct; 32(10):1203–1216. doi: [10.1007/s10822-018-0138-6](https://doi.org/10.1007/s10822-018-0138-6).
- 791 [29] Tielker N, Eberlein L, Güssregen S, Kast SM. The SAMPL6 Challenge on Predicting Aqueous pKa Values from EC-RISM Theory. Journal of
792 Computer-Aided Molecular Design. 2018 Oct; 32(10):1151–1163. doi: [10.1007/s10822-018-0140-z](https://doi.org/10.1007/s10822-018-0140-z).
- 793 [30] Klamt A, Eckert F, Diedenhofen M, Beck ME. First Principles Calculations of Aqueous pK_a Values for Organic and Inorganic Acids Using
794 COSMO-RS Reveal an Inconsistency in the Slope of the pK_a Scale. The Journal of Physical Chemistry A. 2003 Nov; 107(44):9380–9386. doi:
795 [10.1021/jp034688o](https://doi.org/10.1021/jp034688o).
- 796 [31] Eckert F, Klamt A. Accurate Prediction of Basicity in Aqueous Solution with COSMO-RS. Journal of Computational Chemistry. 2006 Jan;
797 27(1):11–19. doi: [10.1002/jcc.20309](https://doi.org/10.1002/jcc.20309).
- 798 [32] Pracht P, Wilcken R, Udvarhelyi A, Rodde S, Grimme S. High Accuracy Quantum-Chemistry-Based Calculation and Blind Prediction of
799 Macroscopic pKa Values in the Context of the SAMPL6 Challenge. Journal of Computer-Aided Molecular Design. 2018 Oct; 32(10):1139–
800 1149. doi: [10.1007/s10822-018-0145-7](https://doi.org/10.1007/s10822-018-0145-7).
- 801 [33] Prasad S, Huang J, Zeng Q, Brooks BR. An Explicit-Solvent Hybrid QM and MM Approach for Predicting pKa of Small Molecules in SAMPL6
802 Challenge. Journal of Computer-Aided Molecular Design. 2018 Oct; 32(10):1191–1201. doi: [10.1007/s10822-018-0167-1](https://doi.org/10.1007/s10822-018-0167-1).
- 803 [34] Robert Fraczkiewicz MW, SAMPL6 pKa Challenge: Predictions of ionization constants performed by the S+pKa method implemented in
804 ADMET Predictor software; February 22, 2018. The Joint D3R/SAMPL Workshop 2018. <https://drugdesigndata.org/about/d3r-2018-workshop>.
- 805 [35] OEMolProp Toolkit 2017.Feb.1.; OpenEye Scientific Software, Santa Fe, NM. <http://www.eyesopen.com>.

Table S1. SMILES and InChI identifiers of SAMPL6 pK_a Challenge molecules. A CSV version of this table can be found in *SAMPL6-supplementary-documents.tar.gz*.

SAMPL6 Molecule ID	Isomeric SMILES	InChI
SM01	c1cc2c(cc1O)c3c(o2)C(=O)NCCC3	InChI=1S/C12H11NO3/c14-7-3-4-10-9(6-7)8-2-1-5-13-12(15)11(8)16-10/h3-4,6,14H,1-2,5H2,(H,13,15)
SM02	c1ccc2c(c1)c(ncn2)Nc3cccc(c3)C(F)(F)	InChI=1S/C15H10F3N3/c16-15(17,18)10-4-3-5-11(8-10)21-14-12-6-1-2-7-13(12)19-9-20-14/h1-9H,(H,19,20,21)
SM03	c1ccc(cc1)Cc2nnnc(s2)NC(=O)c3cccs3	InChI=1S/C14H11N3OS2/c18-13(11-7-4-8-19-11)15-14-17-16-12(20-14)9-10-5-2-1-3-6-10/h1-8H,9H2,(H,15,17,18)
SM04	c1ccc2c(c1)c(ncn2)NCc3ccc(cc3)Cl	InChI=1S/C15H12ClN3/c16-12-7-5-11(6-8-12)9-17-15-13-3-1-2-4-14(13)18-10-19-15/h1-8,10H,9H2,(H,17,18,19)
SM05	c1ccc(c(c1)NC(=O)c2ccc(o2)Cl)N3CCCCC3	InChI=1S/C16H17ClN2O2/c17-15-9-8-14(21-15)16(20)18-12-6-2-3-7-13(12)19-10-4-1-5-11-19/h2-3,6-9H,1,4-5,10-11H2,(H,18,20)
SM06	c1cc2ccnc2c(c1)NC(=O)c3cc(cnc3)Br	InChI=1S/C15H10BrN3O/c16-12-7-11(8-17-9-12)15(20)19-13-5-1-3-10-4-2-6-18-14(10)13/h1-9H,(H,19,20)
SM07	c1ccc(cc1)CNc2c3cccc3ncn2	InChI=1S/C15H13N3/c1-2-6-12(7-3-1)10-16-15-13-8-4-5-9-14(13)17-11-18-15/h1-9,11H,10H2,(H,16,17,18)
SM08	Cc1ccc2c(c1)c(c(c(=O)[nH]2)CC(=O)O)c3cccc3	InChI=1S/C18H15NO3/c1-11-7-8-15-13(9-11)17(12-5-3-2-4-6-12)14(10-16(20)21)18(22)19-15/h2-9H,10H2,1H3,(H,19,22)(H,20,21)
SM09	COc1cccc(c1)Nc2c3cccc3ncn2.Cl	InChI=1S/C15H13N3O.CIH/c1-19-12-6-4-5-11(9-12)18-15-13-7-2-3-8-14(13)16-10-17-15;/h2-10H,1H3,(H,16,17,18);1H
SM10	c1ccc(cc1)C(=O)NCC(=O)Nc2nc3cccc3s2	InChI=1S/C16H13N3O2S/c20-14(10-17-15(21)11-6-2-1-3-7-11)19-16-18-1-2-8-4-5-9-13(12)22-16/h1-9H,10H2,(H,17,21)(H,18,19,20)
SM11	c1ccc(cc1)n2c3c(cn2)c(ncn3)N	InChI=1S/C11H9N5/c12-10-9-6-15-16(11(9)14-7-13-10)8-4-2-1-3-5-8/h1-7H,(H,2,12,13,14)
SM12	c1ccc2c(c1)c(ncn2)Nc3cccc(c3)Cl.Cl	InChI=1S/C14H10ClN3.CIH/c15-10-4-3-5-11(8-10)18-14-12-6-1-2-7-13(12)16-9-17-14;/h1-9H,(H,16,17,18);1H
SM13	Cc1cccc(c1)Nc2c3cc(c(c3ncn2)OC)OC	InChI=1S/C17H17N3O2/c1-11-5-4-6-12(7-11)20-17-13-8-15(21-2)16(22-3)9-14(13)18-10-19-17/h4-10H,1-3H3,(H,18,19,20)
SM14	c1ccc(cc1)n2ncn3c2ccc(c3)N	InChI=1S/C13H11N3/c14-10-6-7-13-12(8-10)15-9-16(13)11-4-2-1-3-5-11/h1-9H,14H2
SM15	c1ccc2c(c1)ncn2c3ccc(cc3)O	InChI=1S/C13H10N2O/c16-11-7-5-10(6-8-11)15-9-14-12-3-1-2-4-13(12)15/h1-9,16H
SM16	c1cc(c(c(c1)Cl)C(=O)Nc2ccncc2)Cl	InChI=1S/C12H8Cl2N2O/c13-9-2-1-3-10(14)11(9)12(17)16-8-4-6-15-7-5-8/h1-7H,(H,15,16,17)
SM17	c1ccc(cc1)CSc2nnc(o2)c3ccncc3	InChI=1S/C14H11N3OS/c1-2-4-11(5-3-1)10-19-14-17-16-13(18-14)12-6-8-15-9-7-12/h1-9H,10H2
SM18	c1ccc2c(c1)c(=O)[nH]c(n2)CCC(=O)Nc3ncc(s3)Cc4ccc(c(c4)F)F	InChI=1S/C21H16F2N4O2S/c22-15-6-5-12(10-16(15)23)9-13-11-24-21(30-13)27-19(28)8-7-18-25-17-4-2-1-3-14(17)20(29)26-18/h1-6,10-11H,7-9H2,(H,24,27,28)(H,25,26,29)
SM19	CCOc1ccc2c(c1)sc(n2)NC(=O)Cc3ccc(c(c3)Cl)Cl	InChI=1S/C17H14Cl2N2O2S/c1-2-23-11-4-6-14-15(9-11)24-17(20-14)21-6(22)8-10-3-5-12(18)13(9)7-10/h3-7,9H,2,8H2,1H3,(H,20,21,22)
SM20	c1cc(cc(c1)OCc2ccc(cc2Cl)Cl)/C=C/3\C(=O)NC(=O)S3	InChI=1S/C17H11Cl2NO3S/c18-12-5-4-11(14(19)8-12)9-23-13-3-1-2-10(6-13)7-15-16(21)20-17(22)24-15/h1-8H,9H2,(H,20,21,22)/b15-7+
SM21	c1cc(cc(c1)Br)Nc2c(cnc(n2)Nc3cccc(c3)Br)F	InChI=1S/C16H11Br2FN4/c17-10-3-1-5-12(7-10)21-15-14(19)9-20-16(23-15)22-13-6-2-4-11(18)8-13/h1-9H,(H,20,21,22,23)
SM22	c1cc2c(cc(c(c2nc1)O))l	InChI=1S/C9H5l2NO/c10-6-4-7(11)9(13)8-5(6)2-1-3-12-8/h1-4,13H
SM23	CCOC(=O)c1ccc(cc1)Nc2cc(cnc(n2)Nc3ccc(cc3)C(=O)OCC)C	InChI=1S/C23H24N4O4/c1-4-30-21(28)16-6-10-18(11-7-16)25-20-14-15(3)24-23(27-20)26-19-12-8-17(9-13-19)22(29)31-5-2/h6-14H,4-5H2,1-3H3,(H2,24,25,26,27)
SM24	COc1ccc(cc1)c2c3c(ncn3oc2c4ccc(cc4)OC)NCCO	InChI=1S/C22H21N3O4/c1-27-16-7-3-14(4-8-16)18-19-21(23-11-12-26)24-13-25-22(19)29-20(18)15-5-9-17(28-2)10-6-15/h3-10,13,26H,11-12H2,1-2H3,(H,23,24,25)

10 Supplementary Information

Microstate ID of Deprotonated State (A)	Microstate ID of Protonated State (HA)	Molecule ID	pKa (exp)	pKa SEM (exp)	pKa ID	Microstate identification source
		SM07	6.08	0.01	SM07_pKa1	NMR measurement
		SM14	5.3	0.01	SM14_pKa2	NMR measurement
		SM14	2.58	0.01	SM14_pKa1	NMR measurement
		SM02	5.03	0.01	SM02_pKa1	Estimated based on SM07 NMR measurement
		SM04	6.02	0.01	SM04_pKa1	Estimated based on SM07 NMR measurement
		SM09	5.37	0.01	SM09_pKa1	Estimated based on SM07 NMR measurement
		SM12	5.28	0.01	SM12_pKa1	Estimated based on SM07 NMR measurement
		SM13	5.77	0.01	SM13_pKa1	Estimated based on SM07 NMR measurement
		SM15	8.94	0.01	SM15_pKa2	Estimated based on SM14 NMR measurement
		SM15	4.7	0.01	SM15_pKa1	Estimated based on SM14 NMR measurement

Figure S1. Dominant microstates of 8 molecules were determined based on NMR measurements. Dominant microstate sequence of 6 derivatives were determined taking SM07 and SM14 as reference. Matched experimental pK_a values were determined by spectrophotometric pK_a measurements [7]. A CSV version of this table can be found in SAMPL6-supplementary-documents.tar.gz.

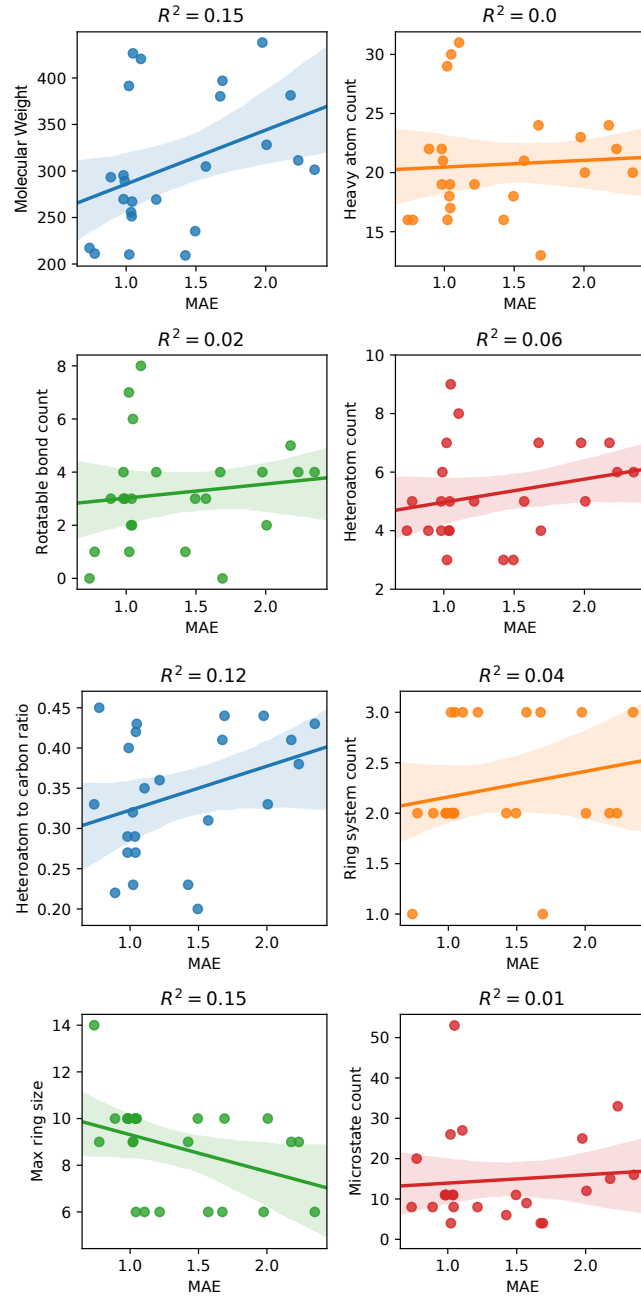


Figure S2. MAE of macroscopic pK_a predictions of each molecule did not show any significant correlation with any molecular descriptor.
 Plots show regression lines, 96% confidence intervals of the regression lines, and R_2 . The following molecular descriptors were calculated using OpenEye OEMolProp Toolkit [35].

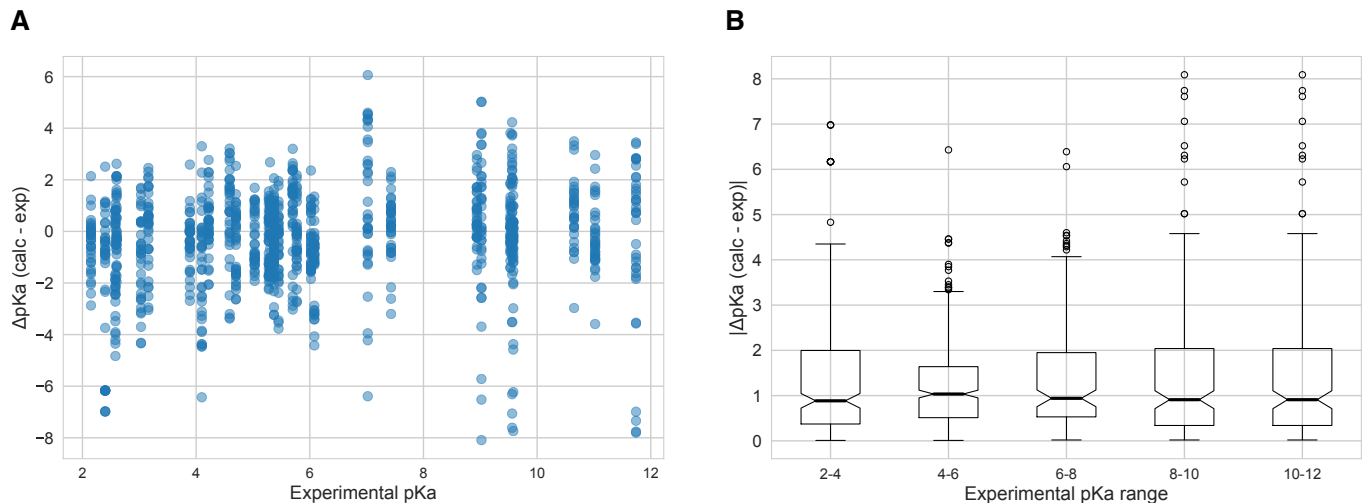


Figure S3. The value of macroscopic pK_a s was not a factor affecting prediction error seen in SAMPL6 Challenge according to the analysis with Hungarian matching. There was not clear trend between pK_a prediction error and the true pK_a error. Very high and very low pK_a values have similar inaccuracy compared to pK_a values close to 7. **A** Scatter plot of macroscopic pK_a prediction error calculated with Hungarian matching vs. experimental pK_a value **B** Box plot of absolute error of macroscopic pK_a predictions binned into 2 pK_a unit intervals of experimental pK_a .

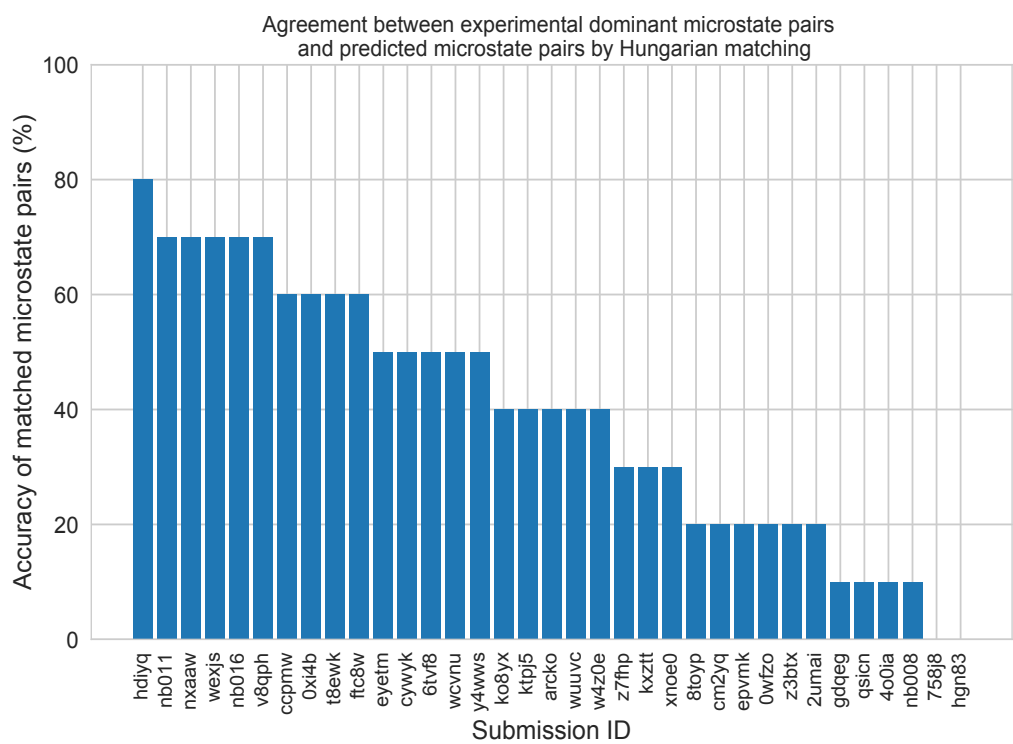


Figure S4. There was low agreement between experimental dominant microstate pairs and the predicted microstate pairs selected by Hungarian algorithm for microscopic pK_a predictions. This analysis could only be performed for 8 molecules with NMR data. Hungarian matching algorithm which matches predicted and experimental values considering only the closeness of the numerical value of pK_a and it often leads to predicted pK_a matches that described a different microstates pair than the experimentally observed dominant microstates..

Table S2. Evaluation statistics calculated for all macroscopic pK_a prediction submissions based on Hungarian match for 24 molecules. Methods are represented via their SAMPL6 submission IDs which can be cross referenced with Table 1 for method details. There are eight error metrics reported: the root-mean-squared error (RMSE), mean absolute error (MAE), mean (signed) error (ME), coefficient of determination (R^2), linear regression slope (m), Kendall's Rank Correlation Coefficient (τ), unmatched experimental pK_as (number of missing pK_a predictions) and unmatched predicted pK_as (number of extra pK_a predictions between 2 and 12. This table is ranked by increasing RMSE. A CSV version of this table can be found in *SAMPL6-supplementary-documents.tar.gz*.

Submission ID	RMSE	MAE	ME	R ²	m	Kendall's Tau	Unmatched exp. pK _a s	Unmatched pred. pK _a s [2,12]
<i>xvxzd</i>	0.68 [0.54, 0.81]	0.58 [0.45, 0.71]	0.24 [-0.01, 0.45]	0.94 [0.88, 0.97]	0.92 [0.84, 1.02]	0.82 [0.68, 0.92]	2	4
<i>gyuhx</i>	0.73 [0.55, 0.91]	0.59 [0.44, 0.74]	0.03 [-0.23, 0.28]	0.93 [0.88, 0.96]	0.98 [0.90, 1.08]	0.88 [0.80, 0.94]	0	7
<i>xmyhm</i>	0.79 [0.52, 1.03]	0.56 [0.38, 0.77]	0.13 [-0.14, 0.41]	0.92 [0.85, 0.97]	0.96 [0.86, 1.08]	0.81 [0.68, 0.90]	0	3
<i>nb017</i>	0.94 [0.72, 1.16]	0.77 [0.58, 0.97]	-0.16 [-0.49, 0.16]	0.88 [0.81, 0.94]	0.94 [0.82, 1.08]	0.73 [0.60, 0.84]	0	6
<i>nb007</i>	0.95 [0.73, 1.15]	0.78 [0.60, 0.97]	0.05 [-0.29, 0.37]	0.88 [0.77, 0.95]	0.84 [0.77, 0.92]	0.79 [0.65, 0.89]	0	13
<i>yqkga</i>	1.01 [0.78, 1.23]	0.80 [0.59, 1.03]	-0.17 [-0.51, 0.19]	0.87 [0.78, 0.93]	0.93 [0.77, 1.08]	0.83 [0.72, 0.91]	0	1
<i>nb010</i>	1.03 [0.77, 1.26]	0.81 [0.61, 1.04]	0.24 [-0.11, 0.59]	0.87 [0.77, 0.94]	0.95 [0.83, 1.08]	0.80 [0.67, 0.90]	0	4
<i>8xt50</i>	1.07 [0.78, 1.36]	0.81 [0.58, 1.07]	-0.47 [-0.82, -0.14]	0.91 [0.84, 0.95]	1.08 [0.94, 1.22]	0.80 [0.68, 0.89]	0	0
<i>nb013</i>	1.10 [0.72, 1.47]	0.80 [0.56, 1.09]	-0.15 [-0.55, 0.22]	0.88 [0.78, 0.95]	1.09 [0.90, 1.25]	0.79 [0.64, 0.90]	0	6
<i>nb015</i>	1.27 [0.98, 1.56]	1.04 [0.80, 1.31]	0.13 [-0.32, 0.56]	0.87 [0.80, 0.93]	1.16 [0.94, 1.34]	0.78 [0.66, 0.86]	0	0
<i>p0jba</i>	1.31 [0.69, 1.73]	1.08 [0.43, 1.72]	-0.92 [-1.72, -0.11]	0.91 [0.51, 1.00]	1.18 [0.36, 1.72]	0.80 [0.00, 1.00]	0	0
<i>37xm8</i>	1.41 [0.93, 1.84]	1.01 [0.68, 1.38]	-0.18 [-0.69, 0.32]	0.83 [0.70, 0.93]	1.16 [0.98, 1.33]	0.70 [0.56, 0.83]	1	1
<i>mkhqa</i>	1.60 [1.13, 2.05]	1.24 [0.90, 1.62]	-0.32 [-0.89, 0.21]	0.80 [0.67, 0.91]	1.14 [0.98, 1.34]	0.64 [0.44, 0.79]	0	6
<i>ttjd0</i>	1.64 [1.20, 2.06]	1.30 [0.96, 1.67]	-0.12 [-0.70, 0.45]	0.81 [0.69, 0.91]	1.2 [1.03, 1.40]	0.65 [0.47, 0.80]	0	5
<i>nb001</i>	1.68 [1.05, 2.37]	1.21 [0.84, 1.68]	0.44 [-0.10, 1.03]	0.80 [0.70, 0.90]	1.16 [0.95, 1.42]	0.72 [0.55, 0.85]	0	7
<i>nb002</i>	1.70 [1.08, 2.38]	1.25 [0.89, 1.70]	0.51 [-0.04, 1.10]	0.80 [0.70, 0.90]	1.15 [0.95, 1.42]	0.72 [0.56, 0.84]	0	7
<i>35bdm</i>	1.72 [0.66, 2.34]	1.44 [0.62, 2.26]	-1.01 [-2.18, 0.13]	0.92 [0.46, 1.00]	1.45 [0.73, 2.15]	0.80 [0.00, 1.00]	0	0
<i>ryzue</i>	1.77 [1.42, 2.12]	1.50 [1.17, 1.84]	1.30 [0.86, 1.72]	0.91 [0.86, 0.95]	1.23 [1.06, 1.41]	0.82 [0.71, 0.91]	0	0
<i>2ii2g</i>	1.80 [1.31, 2.24]	1.39 [1.01, 1.82]	-0.74 [-1.29, -0.15]	0.79 [0.65, 0.89]	1.15 [0.96, 1.37]	0.68 [0.59, 0.82]	0	2
<i>mpwiy</i>	1.82 [1.39, 2.23]	1.48 [1.14, 1.88]	0.10 [-0.54, 0.73]	0.82 [0.70, 0.91]	1.29 [1.12, 1.51]	0.66 [0.49, 0.80]	0	5
<i>5byn6</i>	1.89 [1.50, 2.27]	1.59 [1.24, 1.97]	1.32 [0.84, 1.80]	0.91 [0.85, 0.95]	1.28 [1.10, 1.48]	0.83 [0.72, 0.92]	0	0
<i>y75vj</i>	1.90 [1.50, 2.26]	1.58 [1.21, 1.97]	1.04 [0.46, 1.60]	0.89 [0.79, 0.95]	1.34 [1.16, 1.53]	0.75 [0.57, 0.88]	1	0
<i>w4iyd</i>	1.93 [1.53, 2.28]	1.58 [1.20, 1.98]	1.26 [0.72, 1.76]	0.85 [0.74, 0.92]	1.21 [1.00, 1.40]	0.73 [0.57, 0.85]	0	1
<i>np6b4</i>	1.94 [1.21, 2.71]	1.44 [1.04, 1.94]	-0.47 [-1.08, 0.24]	0.71 [0.60, 0.87]	1.08 [0.81, 1.43]	0.75 [0.62, 0.86]	0	8
<i>nb004</i>	2.01 [1.38, 2.63]	1.57 [1.16, 2.04]	0.56 [-0.10, 1.27]	0.82 [0.72, 0.90]	1.35 [1.15, 1.60]	0.71 [0.54, 0.84]	0	5
<i>nb003</i>	2.01 [1.39, 2.64]	1.58 [1.18, 2.04]	0.52 [-0.14, 1.22]	0.82 [0.73, 0.91]	1.36 [1.16, 1.61]	0.71 [0.54, 0.84]	0	5
<i>yc70m</i>	2.03 [1.73, 2.33]	1.80 [1.48, 2.13]	-0.41 [-1.09, 0.31]	0.47 [0.28, 0.64]	0.56 [0.35, 0.83]	0.53 [0.35, 0.68]	0	27
<i>hytjn</i>	2.16 [1.24, 3.06]	1.39 [0.86, 2.04]	0.71 [0.03, 1.48]	0.45 [0.13, 0.78]	0.62 [0.26, 1.00]	0.47 [0.16, 0.73]	1	27
<i>f0gew</i>	2.18 [1.38, 2.95]	1.58 [1.09, 2.16]	-0.73 [-1.42, 0.04]	0.77 [0.67, 0.89]	1.29 [1.01, 1.63]	0.76 [0.63, 0.86]	0	0
<i>q3pfp</i>	2.19 [1.33, 3.09]	1.51 [0.99, 2.13]	0.59 [-0.10, 1.37]	0.44 [0.13, 0.77]	0.66 [0.27, 1.07]	0.50 [0.20, 0.75]	1	22
<i>ds62k</i>	2.22 [1.62, 2.81]	1.78 [1.34, 2.27]	0.78 [0.06, 1.52]	0.82 [0.70, 0.90]	1.41 [1.20, 1.63]	0.72 [0.55, 0.85]	0	4
<i>xikp8</i>	2.35 [1.94, 2.73]	2.06 [1.66, 2.47]	0.77 [-0.02, 1.58]	0.89 [0.80, 0.95]	1.59 [1.40, 1.81]	0.76 [0.59, 0.89]	1	0
<i>nb005</i>	2.38 [1.79, 2.95]	1.91 [1.44, 2.43]	0.31 [-0.49, 1.15]	0.84 [0.74, 0.91]	1.56 [1.34, 1.82]	0.71 [0.54, 0.83]	0	0
<i>5nm4j</i>	2.45 [1.42, 3.34]	1.58 [0.94, 2.34]	0.05 [-0.80, 1.07]	0.19 [0.00, 0.70]	0.40 [-0.06, 0.81]	0.34 [-0.04, 0.67]	4	1
<i>ad5pu</i>	2.54 [1.68, 3.30]	1.83 [1.24, 2.49]	-0.65 [-1.48, 0.25]	0.76 [0.64, 0.88]	1.43 [1.12, 1.78]	0.77 [0.63, 0.88]	0	0
<i>pwn3m</i>	2.60 [1.45, 3.53]	1.54 [0.83, 2.37]	0.79 [-0.06, 1.77]	0.21 [0.00, 0.63]	0.37 [0.01, 0.78]	0.34 [0.04, 0.63]	1	3
<i>nb006</i>	2.98 [2.37, 3.56]	2.53 [2.00, 3.10]	0.42 [-0.60, 1.47]	0.84 [0.74, 0.92]	1.78 [1.55, 2.06]	0.71 [0.54, 0.84]	0	0
<i>0hxtm</i>	3.26 [1.81, 4.39]	1.92 [1.03, 2.98]	1.38 [0.37, 2.56]	0.08 [0.00, 0.48]	0.28 [-0.17, 0.83]	0.29 [-0.04, 0.61]	3	7

Table S3. Evaluation statistics calculated for all microscopic pK_a prediction submissions based on Hungarian match for 8 molecules with NMR data. Methods are represented via their SAMPL6 submission IDs which can be cross referenced with Table 1 for method details. There are eight error metrics reported: the root-mean-squared error (RMSE), mean absolute error (MAE), mean (signed) error (ME), coefficient of determination (R^2), linear regression slope (m), Kendall's Rank Correlation Coefficient (τ), unmatched experimental pK_as (number of missing pK_a predictions) and unmatched predicted pK_as (number of extra pK_a predictions between 2 and 12. This table is ranked by increasing RMSE. A CSV version of this table can be found in *SAMPL6-supplementary-documents.tar.gz*.

Submission ID	RMSE	MAE	ME	R ²	m	Kendall's Tau	Unmatched exp. pK _a s	Unmatched pred. pK _a s [2,12]
nb011	0.47 [0.30, 0.64]	0.33 [0.22, 0.46]	-0.02 [-0.18, 0.14]	0.97 [0.94, 0.99]	1.01 [0.97, 1.06]	0.90 [0.78, 0.96]	0	36
hdlyq	0.62 [0.47, 0.76]	0.47 [0.33, 0.62]	0.13 [-0.09, 0.34]	0.95 [0.92, 0.97]	0.34 [0.92, 1.09]	0.87 [0.79, 0.93]	0	16
epvmk	0.63 [0.43, 0.81]	0.47 [0.32, 0.63]	-0.02 [-0.25, 0.21]	0.95 [0.89, 0.98]	0.21 [0.91, 1.04]	0.81 [0.68, 0.91]	0	37
xnoe0	0.65 [0.47, 0.82]	0.50 [0.36, 0.66]	-0.1 [-0.32, 0.13]	0.95 [0.89, 0.98]	0.13 [0.92, 1.05]	0.82 [0.69, 0.91]	0	36
gdqeg	0.65 [0.41, 0.89]	0.43 [0.27, 0.62]	0.11 [-0.10, 0.35]	0.94 [0.88, 0.98]	0.35 [0.87, 1.02]	0.83 [0.67, 0.95]	0	53
400ia	0.66 [0.44, 0.86]	0.47 [0.31, 0.64]	0.00 [-0.22, 0.24]	0.94 [0.88, 0.98]	0.24 [0.87, 1.05]	0.85 [0.73, 0.94]	0	35
nb008	0.76 [0.48, 1.02]	0.52 [0.34, 0.73]	-0.08 [-0.37, 0.17]	0.93 [0.85, 0.98]	0.17 [0.79, 0.93]	0.84 [0.73, 0.92]	0	35
ccpmw	0.79 [0.62, 0.94]	0.62 [0.46, 0.80]	-0.17 [-0.44, 0.11]	0.92 [0.86, 0.96]	0.11 [0.82, 1.05]	0.80 [0.67, 0.89]	0	7
0xi4b	0.84 [0.58, 1.07]	0.61 [0.42, 0.83]	0.22 [-0.07, 0.51]	0.92 [0.84, 0.97]	0.51 [0.91, 1.09]	0.81 [0.65, 0.92]	0	32
cwyk	0.86 [0.60, 1.10]	0.62 [0.42, 0.84]	0.13 [-0.16, 0.44]	0.90 [0.82, 0.96]	0.44 [0.86, 1.08]	0.81 [0.64, 0.92]	0	35
ftc8w	0.86 [0.51, 1.17]	0.59 [0.39, 0.83]	0.10 [-0.19, 0.41]	0.90 [0.77, 0.97]	0.41 [0.84, 0.98]	0.75 [0.57, 0.88]	0	35
nxaaw	0.89 [0.56, 1.25]	0.61 [0.41, 0.87]	-0.02 [-0.35, 0.28]	0.89 [0.75, 0.97]	0.28 [0.85, 1.00]	0.79 [0.63, 0.91]	0	29
nb016	0.95 [0.71, 1.18]	0.77 [0.57, 0.98]	-0.23 [-0.56, 0.12]	0.89 [0.83, 0.95]	0.12 [0.82, 1.07]	0.75 [0.62, 0.85]	0	3
kxzt	0.96 [0.56, 1.33]	0.64 [0.41, 0.92]	0.00 [-0.32, 0.36]	0.90 [0.76, 0.97]	0.36 [0.96, 1.13]	0.79 [0.63, 0.91]	0	37
eyetm	0.98 [0.69, 1.27]	0.72 [0.50, 0.97]	-0.32 [-0.65, 0.00]	0.91 [0.86, 0.96]	0.00 [0.94, 1.22]	0.78 [0.64, 0.88]	0	7
cm2yq	0.99 [0.44, 1.54]	0.56 [0.31, 0.90]	0.10 [-0.21, 0.50]	0.91 [0.83, 0.98]	0.50 [0.96, 1.25]	0.89 [0.80, 0.96]	0	36
2umai	1.00 [0.46, 1.54]	0.57 [0.33, 0.91]	0.07 [-0.25, 0.46]	0.91 [0.82, 0.98]	0.46 [0.96, 1.26]	0.87 [0.76, 0.95]	0	36
ko8yx	1.01 [0.76, 1.25]	0.78 [0.56, 1.01]	0.35 [0.01, 0.67]	0.91 [0.82, 0.96]	0.67 [0.96, 1.19]	0.78 [0.64, 0.89]	0	26
wuuvc	1.02 [0.51, 1.53]	0.62 [0.38, 0.93]	0.19 [-0.13, 0.58]	0.88 [0.80, 0.96]	0.58 [0.85, 1.19]	0.90 [0.81, 0.96]	0	36
ktpj5	1.02 [0.51, 1.56]	0.61 [0.37, 0.95]	0.17 [-0.16, 0.57]	0.88 [0.80, 0.96]	0.57 [0.87, 1.22]	0.89 [0.80, 0.96]	0	36
z7fhp	1.02 [0.49, 1.55]	0.61 [0.36, 0.94]	0.08 [-0.24, 0.48]	0.90 [0.82, 0.97]	0.48 [0.97, 1.26]	0.88 [0.80, 0.95]	0	28
arcko	1.04 [0.73, 1.32]	0.77 [0.53, 1.02]	0.37 [0.05, 0.72]	0.89 [0.80, 0.94]	0.72 [0.90, 1.14]	0.78 [0.62, 0.90]	0	24
y4wws	1.04 [0.70, 1.33]	0.74 [0.49, 1.00]	-0.31 [-0.66, 0.05]	0.91 [0.85, 0.96]	0.05 [1.02, 1.26]	0.79 [0.68, 0.88]	0	30
wcvnu	1.11 [0.80, 1.39]	0.84 [0.59, 1.11]	0.28 [-0.10, 0.66]	0.89 [0.77, 0.95]	0.66 [0.98, 1.22]	0.73 [0.54, 0.88]	1	27
8toyp	1.13 [0.61, 1.65]	0.70 [0.42, 1.05]	0.13 [-0.25, 0.56]	0.88 [0.81, 0.96]	0.56 [0.98, 1.29]	0.83 [0.72, 0.92]	0	27
qsicn	1.17 [0.30, 1.65]	0.88 [0.23, 1.54]	-0.76 [-1.54, 0.01]	0.91 [0.46, 1.00]	0.01 [0.52, 1.59]	0.80 [0.00, 1.00]	0	2
wexjs	1.30 [0.95, 1.62]	0.98 [0.68, 1.29]	0.27 [-0.17, 0.74]	0.86 [0.74, 0.93]	0.74 [1.00, 1.29]	0.73 [0.55, 0.86]	0	25
v8qph	1.37 [0.92, 1.79]	0.98 [0.66, 1.34]	-0.15 [-0.64, 0.34]	0.84 [0.70, 0.93]	0.34 [0.97, 1.32]	0.70 [0.55, 0.82]	0	6
w420e	1.57 [1.18, 1.94]	1.23 [0.90, 1.58]	0.09 [-0.48, 0.62]	0.85 [0.76, 0.91]	0.62 [1.08, 1.46]	0.72 [0.60, 0.82]	0	19
6tvf8	1.88 [0.87, 2.85]	1.02 [0.54, 1.66]	0.45 [-0.14, 1.18]	0.51 [0.16, 0.87]	1.18 [0.26, 0.89]	0.61 [0.34, 0.82]	0	55
0wfzo	2.89 [1.73, 3.89]	1.88 [1.17, 2.68]	0.76 [-0.15, 1.77]	0.48 [0.21, 0.75]	1.77 [0.60, 1.37]	0.51 [0.30, 0.70]	0	4
t8ewk	3.30 [1.89, 4.39]	1.98 [1.06, 3.00]	1.32 [0.27, 2.49]	0.07 [0.00, 0.45]	2.49 [-0.17, 0.79]	0.28 [-0.03, 0.6]	0	6
z3btx	4.00 [2.30, 5.45]	2.49 [1.47, 3.65]	1.48 [0.26, 2.86]	0.29 [0.04, 0.60]	2.86 [0.31, 1.44]	0.43 [0.19, 0.63]	0	1
758j8	4.52 [2.64, 6.18]	2.95 [1.85, 4.25]	1.85 [0.48, 3.38]	0.24 [0.02, 0.58]	3.38 [0.20, 1.51]	0.34 [0.08, 0.57]	0	2
hgn83	6.38 [4.04, 8.47]	4.11 [2.52, 5.93]	2.13 [0.07, 4.28]	0.08 [0.00, 0.39]	4.28 [-0.18, 1.43]	0.32 [0.07, 0.56]	0	0

Table S4. Evaluation statistics calculated for all microscopic pK_a prediction submissions based on microstate pair match for 8 molecules with NMR data. Methods are represented via their SAMPL6 submission IDs which can be cross referenced with Table 1 for method details. There are eight error metrics reported: the root-mean-squared error (RMSE), mean absolute error (MAE), mean (signed) error (ME), coefficient of determination (R^2), linear regression slope (m), Kendall's Rank Correlation Coefficient (τ), unmatched experimental pK_as (number of missing pK_a predictions) and unmatched predicted pK_as (number of extra pK_a predictions between 2 and 12. This table is ranked by increasing RMSE. A CSV version of this table can be found in *SAMPL6-supplementary-documents.tar.gz*.

Update this table with dominant microstate accuracy

Submission ID	RMSE	MAE	ME	R^2	m	Kendall's Tau	Unmatched exp. pK _a s	Unmatched pred. pK _a s [2,12]
nb016	0.52 [0.25, 0.71]	0.43 [0.23, 0.65]	-0.09 [-0.45, 0.30]	0.92 [0.05, 0.99]	0.99 [0.14, 1.16]	0.62 [-0.14, 1.00]	0	3
hdlyq	0.68 [0.49, 0.83]	0.60 [0.39, 0.80]	0.38 [0.02, 0.70]	0.86 [0.47, 0.98]	0.91 [0.45, 1.26]	0.78 [0.4, 1.00]	0	16
nb011	0.72 [0.35, 1.07]	0.54 [0.28, 0.86]	0.45 [0.14, 0.83]	0.86 [0.18, 0.98]	0.93 [0.50, 1.21]	0.64 [0.26, 0.95]	0	36
ftc8w	0.75 [0.52, 0.96]	0.68 [0.50, 0.89]	-0.31 [-0.68, 0.16]	0.87 [0.02, 0.99]	1.12 [-0.11, 1.39]	0.56 [-0.10, 1.00]	0	35
6tvf8	0.76 [0.55, 0.95]	0.68 [0.46, 0.90]	-0.63 [-0.89, -0.35]	0.92 [0.78, 0.99]	0.94 [0.69, 1.41]	0.87 [0.6, 1.00]	0	55
t8ewk	0.96 [0.65, 1.19]	0.81 [0.46, 1.13]	-0.77 [-1.12, -0.38]	0.80 [0.53, 0.96]	0.96 [0.76, 2.26]	0.78 [0.31, 1.00]	1	7
v8qph	0.99 [0.40, 1.52]	0.67 [0.29, 1.17]	-0.09 [-0.75, 0.45]	0.68 [0.11, 0.97]	0.96 [-1.26, 1.16]	0.38 [-0.3, 1.00]	0	6
ccpmw	1.07 [0.78, 1.27]	0.95 [0.60, 1.25]	-0.83 [-1.25, -0.37]	0.74 [0.43, 0.99]	0.95 [0.70, 2.32]	0.89 [0.52, 1.00]	1	8
0xi4b	1.15 [0.75, 1.50]	0.98 [0.63, 1.36]	-0.30 [-0.94, 0.44]	0.77 [0.02, 0.98]	1.26 [0.09, 2.10]	0.51 [-0.14, 1.00]	0	33
cywyk	1.17 [0.88, 1.41]	1.06 [0.74, 1.35]	-0.47 [-1.09, 0.24]	0.73 [0.02, 0.98]	1.15 [-0.04, 2.00]	0.56 [-0.08, 1.00]	0	36
eyetm	1.17 [0.77, 1.52]	1.00 [0.61, 1.41]	-0.89 [-1.38, -0.38]	0.67 [0.30, 0.94]	0.93 [0.65, 2.59]	0.72 [0.29, 1.00]	1	8
nb008	1.26 [0.74, 1.71]	1.09 [0.63, 1.57]	0.47 [-0.40, 1.32]	0.79 [0.01, 0.99]	1.21 [-0.59, 1.85]	0.52 [-0.2, 1.00]	0	38
y4wws	1.41 [0.95, 1.80]	1.22 [0.78, 1.66]	-0.71 [-1.44, 0.06]	0.87 [0.05, 0.98]	1.55 [0.41, 2.02]	0.56 [-0.11, 1.00]	0	31
ktpj5	1.46 [0.83, 2.10]	1.15 [0.67, 1.77]	0.94 [0.29, 1.68]	0.77 [0.01, 0.98]	1.28 [-0.26, 1.60]	0.42 [-0.27, 0.95]	0	37
wuuvc	1.47 [0.84, 2.09]	1.18 [0.70, 1.77]	0.99 [0.36, 1.68]	0.78 [0.01, 0.98]	1.27 [-0.24, 1.58]	0.47 [-0.20, 1.00]	0	37
xnoe0	1.54 [1.09, 2.00]	1.39 [1.02, 1.83]	0.91 [0.11, 1.64]	0.82 [0.01, 0.98]	1.47 [-0.30, 1.79]	0.42 [-0.27, 0.95]	0	37
qsicn	1.58 [1.44, 1.70]	1.57 [1.44, 1.70]	-1.57 [-1.7, -1.44]	1.00 [0.00, 1.00]	1.06		0	2
epvmk	1.66 [1.20, 2.15]	1.50 [1.07, 1.96]	1.12 [0.31, 1.82]	0.82 [0.02, 0.98]	1.47 [-0.21, 1.8]	0.42 [-0.25, 0.95]	0	37
400ia	1.73 [1.33, 2.17]	1.62 [1.29, 2.02]	1.31 [0.53, 1.93]	0.87 [0.03, 0.99]	1.50 [0.07, 1.84]	0.56 [-0.07, 1.00]	0	36
ko8yx	1.75 [1.08, 2.45]	1.44 [0.87, 2.12]	1.38 [0.74, 2.10]	0.97 [0.88, 1.00]	1.66 [1.46, 2.28]	0.91 [0.69, 1.00]	0	27
2umai	1.76 [1.21, 2.35]	1.54 [1.04, 2.11]	1.31 [0.55, 2.03]	0.82 [0.02, 0.98]	1.43 [-0.02, 1.77]	0.47 [-0.17, 0.95]	0	37
cm2yq	1.77 [1.22, 2.36]	1.55 [1.06, 2.12]	1.33 [0.57, 2.04]	0.82 [0.02, 0.98]	1.43 [-0.02, 1.76]	0.47 [-0.17, 0.95]	0	37
nxaaw	1.80 [0.84, 2.80]	1.34 [0.80, 2.18]	0.16 [-0.77, 1.41]	0.59 [0.02, 0.97]	1.37 [-0.08, 2.92]	0.6 [-0.05, 1.00]	0	30
wcvnu	1.90 [1.14, 2.64]	1.57 [0.97, 2.27]	1.44 [0.70, 2.24]	0.97 [0.91, 1.00]	1.78 [1.58, 2.48]	0.91 [0.69, 1.00]	0	27
kxzt	2.00 [1.13, 2.73]	1.64 [1.00, 2.39]	1.64 [1.00, 2.39]	0.83 [0.01, 0.98]	1.42 [-0.21, 1.99]	0.56 [-0.10, 1.00]	0	38
wexjs	2.05 [1.18, 2.93]	1.66 [1.01, 2.47]	1.48 [0.63, 2.39]	0.96 [0.55, 0.99]	1.87 [1.54, 2.29]	0.73 [0.20, 1.00]	0	26
z7fhp	2.14 [1.38, 2.87]	1.80 [1.12, 2.58]	1.28 [0.18, 2.34]	0.78 [0.02, 0.98]	1.71 [-0.41, 2.13]	0.42 [-0.25, 0.95]	0	30
gdqeg	2.38 [1.97, 2.71]	2.25 [1.74, 2.68]	-1.61 [-2.46, -0.37]	0.10 [0.00, 0.98]	0.31 [-0.60, 1.63]	0.29 [-0.45, 1.00]	0	53
8toyp	2.63 [1.89, 3.29]	2.34 [1.59, 3.07]	1.78 [0.47, 2.89]	0.82 [0.02, 0.98]	1.94 [-0.06, 2.39]	0.47 [-0.17, 0.95]	0	29
w420e	2.63 [1.81, 3.53]	2.34 [1.67, 3.18]	1.74 [0.46, 2.92]	0.98 [0.55, 1.00]	2.28 [1.52, 2.41]	0.73 [0.20, 1.00]	0	20
arcko	2.64 [1.23, 3.78]	2.08 [1.10, 3.24]	1.71 [0.44, 3.10]	0.57 [0.04, 0.95]	1.42 [0.56, 2.93]	0.56 [-0.06, 1.00]	0	28
0wfzo	18.72 [11.21, 25.03]	15.80 [9.9, 22.35]	15.09 [8.28, 22.12]	0.09 [0.01, 0.73]	2.35 [-10.18, 8.12]	0.02 [-0.65, 0.66]	0	12
z3btv	22.60 [15.03, 29.00]	19.70 [12.97, 26.69]	19.70 [12.97, 26.69]	0.09 [0.01, 0.72]	2.35 [-10.00, 8.28]	0.02 [-0.66, 0.66]	0	7
758j8	23.76 [16.33, 30.24]	21.00 [14.26, 28.00]	21.00 [14.26, 28.00]	0.09 [0.01, 0.71]	2.35 [-10.34, 8.12]	0.02 [-0.65, 0.65]	0	8
hgn83	27.91 [20.54, 34.52]	25.60 [18.9, 32.64]	25.60 [18.9, 32.64]	0.09 [0.01, 0.72]	2.35 [-10.21, 8.00]	0.02 [-0.65, 0.65]	0	5